CALIFORNIA STATE UNIVERSITY, NORTHRIDGE

Performance Characterization of Range Finding Sensors

A graduate project submitted in partial fulfillment of the requirements

For the degree of Master of Science in Electrical Engineering

By

Caleb Alvin Amposta

December 2020

The graduate project of Caleb Alvin Amposta is approved:

_____	_____
Dr. Shahnam Mirzaei	Date
_____	_____
Dr. Xiyi Hang	Date
_____	_____
Dr. Xiaojun Geng, Chair	Date

California State University, Northridge

Table of Contents

List of Tables

List of Figures

Abstract

Performance Characterization of Range Finding Sensors

By
Caleb Amposta
Master of Science in Electrical Engineering

The performance characterization of range finding sensors were a preliminary phase of the sensor integration process as part of the initial work to complete the *Drone Modular Smart Pallet* project. The sensor was the MB1242, I2CXL-MaxSonar-EZ4 ultrasonic sensor. The data was collected with the processing of the Raspberry Pi 4B microcomputer and analyzed in MATLAB. The project was split into four parts: collecting sensor data, analyzing the external factors affecting the sensor performance, building a model from the sensor measurements, and preliminary processing of the range readings using a moving average, median, and Kalman filter. The most significant performance factors were highlighted for consideration in the pallets future sensor fusion process. Compensation for changing wave propagation speeds in varying temperatures was implemented in real time to evaluate potential performance improvements. A simulation was done for range-finding in flight to evaluate the effectiveness of several noise filtering methods. Real data was used whenever possible for the cases of range finding a stationary target on a static platform.

Chapter 1: Introduction

With a market demanding an increase of faster transportation of people and freight, autonomous aerial vehicles have begun to take to the sky. Compared to the simpler wheeled robotic vehicles, aerial vehicles travel with six degrees of freedom. The vertical dimension increases complexity because few sensors are able to determine 3D position in space accurately. One way to solve this issue is the fusion of multiple sensors to create a picture of the surroundings. The sensing of objects to create the picture of the environment surrounding the vehicle can be used for collision avoidance and route planning. This is all imperative in improving, speed, efficiency, and most importantly safety as more vehicles take flight to deliver their shipments. Several tasks must be completed in order to have a fully integrated suite of sensors including using the sensors, examining their behavior, and developing methods to improve their performance when integrated with other components. This report is an exposition on one aspect of the sensor characterization milestone with an emphasis on ultrasonic sensors where the end goal is to increase the use and confidence in autonomous aerial vehicles in daily life.

The second chapter of this report examines the origin of the project including the big picture goals in the context of Advanced Air Mobility and how range finding sensors on the Drone Modular Smart Pallet (DroneMSP) are required in the process. It also covers the foundations of how range finding sensors operate including the physical factors that specifically affect ultrasonic performance. Lastly, it lays out all of the main and sub-objectives in completing the project.

The third chapter provides a review of the literature relevant to this project. Several models are proposed that could approximate the sensor behavior. An examination of modern methods of filtering noise are outlined for improving the sensor performance.

The focus of the next chapter are the experiments and raw sensor data collected. The test setup, conditions, and limitations are outlined. Processed data is presented for analyzing the change in performance based on each individual factor. The raw sensor data is then used to approximate a generic sensor model. Each subsection is concluded with a proposal on future work/further testing that could be accomplished to systematically analyze the behavior of other range finding sensors.

The results from chapter four are the basis for improving performance in chapter five by adding temperature-based coefficient correction and noise reduction methods. The implementation of a simple temperature compensator was completed on real-time sensor data with the ranging performance compared to the baseline. The next section of the chapter advances the project by investigating further improvements that can be made by reducing noise from the factors discussed in chapter four. A mixed density noise model was assumed and applied to the raw sensor data. Several modern noise filtering techniques were then chosen and simulated against additive gaussian noise to discover the potential performance trade-offs. This last chapter propels the project for future research and preparation for when the range finding sensors are integrated onto the modular smart pallet.

Chapter 2: Background

2.1 Drone Modular Smart Pallet

The Drone Modular Smart Pallet (DroneMSP) is one potential component of NASAs Advanced Air Mobility campaign to "develop an air transportation system that moves people and cargo between places previously not served or underserved by aviation – local, regional, intraregional, urban"[2]. The Drone MSP's purpose is to collect real-time flight data for developing sensor models and algorithms for flight control that could equip any aerial vehicle to make it autonomous. The initial prototype is to be equipped with microprocessors, a large array of sensors for data recording, and online sensor fusion. The four main tasks in completing the DroneMSP project were broken down as: Data Acquisition System Development, Sensor Characterization and Signal Processing, Smart Pallet Mechanical Design and Development, and Plug-and-Play Interfacing Unit Development. The sensors and their interface/connection with the pallet processor were identified in [1]. This project falls under task 2 with data analysis of the sensor behavior enabling a better understanding of how these sensors will operate when in flight by characterizing their baseline performance.

2.2 Fundamental Theory of Range Finding Sensors

Aerial vehicles can utilize many sensors to perform their mission including inertial measurement units (IMU), barometers, global positioning systems (GPS), rangefinders, magnetometers, etc. Rangefinders specifically can serve two purposes: sensing the ground for landing, sensing obstacles in the flight path for avoidance. Many rangefinders operate on the same fundamental principal of transmitting a wave in the direction of an object and counting the time it takes for the reflection of that wave off of an object (echo) to return. The three remote sensing technologies many people have heard of that use this principle is radar, lidar, and sonar (or ultrasonic which is

the same concept as sonar except it uses a wave that is a higher frequency than a human can hear). The composition of the transmitted waves that differentiate these technologies are actually revealed in the first word of the acronyms that they come from: Radar-Radio Detection And Ranging, Lidar-Light Detection And Ranging, and Sonar-Sound Navigation And Ranging. A very basic mathematical equation can be used to describe how these sensors operate. Radio and light waves are both forms of electromagnetic energy. It is known that electromagnetic energy travels in free space at the speed of light which is $3x10^8$ m/s. Therefore, the time it takes for the wave to travel from the transmitter and return to the receiver (assuming they are collocated) is twice the range divided by the speed of travel. Reworking that relationship is shown in (1)

$$R = \frac{cTof}{2} \tag{1}$$

where R is the range, c is the speed of light, and Tof is the time for the signal to travel to the target and back. Ultrasonic sensors operate with the same equation except the propagation speed of ultrasonic waves is 1540 m/s, much slower than the speed of light.

2.3 External Factors Affecting Range Finding Performance

The waves that are reflected off of the object a range finder is sensing can be quantified by a minimum detectable strength/intensity that their receiver can pick up. Additionally, sensors may produce data that is noisy or spurious because of what they receive in their operating vicinity. There are several factors that may affect performance of a range finding sensors either by producing noise or attenuating the resultant signal echo. For ultrasonic sensors, the signal power of an acoustic wave is attenuated according to the inverse square law [9]. Since the transmission and reflection are both isotropic, the $4\pi R^2$ term must be accounted for twice. The intensity of the acoustic signal is also affected by absorption of the medium and the frequency of the signal [9].

These elements can be summarized into one equation that describes the intensity at a transceiver reception from range R.

$$I = \frac{I_{max} e^{-2\alpha R}}{16\pi R^4} \quad (2)$$

where I_{max} is the initial intensity, α is the attenuation coefficient for the medium, R is the range, and I is the intensity at the range. This element of ultrasonic sensors drives testing at many different ranges to determine the precision and accuracy i.e. the fundamental measures of ultrasonic sensor performance.

The ultrasonic pulses emitted from range finders traditionally radiate in a conical type beam pattern. The beam pattern describes the sensitivity at different spatial angles. The beam patterns are generally equal in the transmitter and receiver. Properties of the conical pattern are: peak sound pressure at the center of the beam, characterized by the -3dB beam angle around the peak i.e. sound pressure reduces to half, and side lobes at 20db down from the peak. The radiation pattern for a flat, circular piston source transducer was captured in [15] by the equation

$$P_{dB}(\theta) = 20 \log \left[\frac{2J_1\left(\frac{\pi D}{\lambda}\right) sin(\theta)}{\left(\frac{\pi D}{\lambda}\right) sin(\theta)} \right] \quad (3)$$

where θ is the angle of the sound pressure from an axis perpendicular to the center of the piston, D is the diameter of the piston, λ is the wavelength of the sound, and J_1 is the first order Bessel Function. The radiation pattern also referred to as the beam spread has several implications on range finding performance. A narrow beam improves total detection range as more of the concentrated energy will reflect back to the receiver. The trade-off is that more sensors are required to cover a large area. Furthermore, larger beam patterns are more effective for multi-

surface targets. A target perfectly normal to the sensor will reflect almost all energy back towards the sensor (see reflectivity/absorption in the next section). Uneven surfaces cause the sound waves to reflect in different directions. A large beam spread on an uneven surface increases the chances that some ultrasonic energy will be reflected back to the receiver.

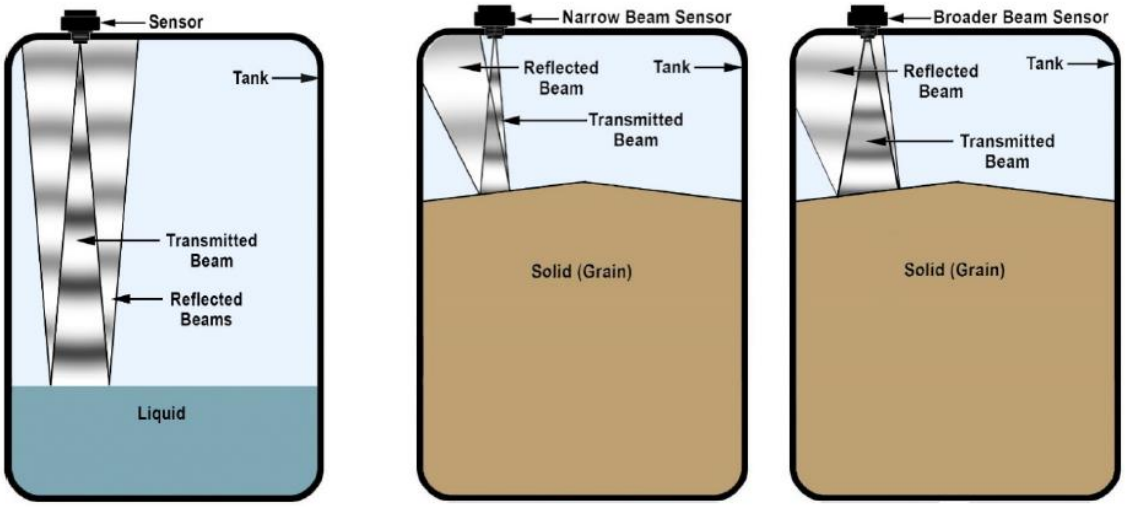

Figure 2.1 How Beam Spread Affects Detection of Uneven Surfaces (Massa, [15])

The beam spread from the range finder can be characterized by finding the field-of-view i.e. maximum incidence angles in which the sensor is able to detect ultrasonic energy. This drives testing where the range finding sensor is rotated away from the point where the shortest distance to the target is normal to the target's surface.

When transmitted ultrasonic energy strikes a target at the acoustic interface i.e. boundary where materials of different acoustic impedances meet such as air and concrete, some of the energy is reflected back to the transmitter while the rest of the energy is absorbed [10]. The amount of energy reflected back is dependent on the reflectivity of the material which is a function of the acoustic impedance mismatch between the medium and target materials. This relationship is the reflection coefficient described in (4).

$$\Gamma_R = \left[\frac{Z_m - Z_T}{Z_m + Z_T}\right]^2 = \frac{I_R}{I_I} \quad (4)$$

where Γ_R is the reflection coefficient, Z_m is the acoustic impedance of the medium in which it travels e.g. air, and Z_t is the acoustic impedance of the target. It is also described as the reflected intensity, I_R, over the incident intensity, I_I. Accounting for the reflectivity in the numerator results in a new intensity equation in (5).

$$I = \frac{\Gamma_R I_{max} e^{-2\alpha R}}{16\pi R^4} \quad (5)$$

Aerial vehicles such as the DroneMSP in this application will land on a variety of materials depending on location including rooftops, helipads, runways, open fields, etc. where each has a different reflectivity. This drives testing of the sensor performance for a multitude of materials such as concrete, wood, and asphalt.

Outdoor operation of range finding sensors implies that the sensor will be exposed to changing temperatures. The range calculation in (1) depends on a constant speed of sound. However, the speed of sound changes with temperature and is directly proportional to the square root of the temperature. This is because the wave propagation speed is a function of density and volume modulus which are both temperature dependent [10]. The equation for speed of sound based on temperature is shown in (6).

$$v = \sqrt{\frac{\gamma RT}{M}} \quad (6)$$

Where γ is the adiabatic constant of the specific gas, R is the universal gas constant, T is the absolute temperature, and M is the molecular mass of the gas. The ultrasonic range finding

sensors, if not equipped with a temperature sensor, are usually calibrated for a set temperature such as room temperature e.g. 20° C/68° F. Compensation can be achieved to adjust sensor measurements based on the speed of sound changing due to temperature. This is described in the equation relating the calibration and true temperature in (7).

$$R_T = R_m \sqrt{\frac{T_T}{T_C}} \tag{7}$$

where T_C and T_T are the calibrated and true temperatures and R_M and R_T are the measured and true ranges. The compensation shows that measurements taken in colder temperatures yield a range longer than the true range and measurements in warmer temperatures will report a range shorter than the true range. Temperature dependent range finders drive testing of the performance for an array of potential temperatures the sensor may be exposed to in an operational environment.

The last factor effecting range finding sensors that this paper examines is interference from other transmitters both external and internal to the system. As alluded to previously, operating range finding sensors outdoors makes them naturally susceptible to their environment. Several recent studies [[16] found that very high frequency sound waves can be found in numerous different places including Public Address Voice Alarms (PAVA), pest deterrent devices, hand dryers, proximity sensors, CRT televisions, and more. The end goal of operating the DroneMSP in an everyday environment means these sources must be considered. Internal interference, or crosstalk, occurs when a returning ultrasonic sound pulse is received by a system that was not the original transmitter, likely resulting in errors. As is the case with the DroneMSP, multiple ultrasonic range finders will be used to cover sectors that create a “viewing area” underneath the aerial vehicle which means near simultaneous transmission is necessary to complete its

objectives. The range finding sensors must be configured in either of two ways to avoid cross talk: synchronized where all sensors transmit pulses at the same time or multiplexed where sensors operate sequentially such that the next sensor to transmit waits for the previous sensor to finish ranging. Sensors operating in a free run mode where they are not synchronized or multiplexed are vulnerable to crosstalk unless positioned to face opposite directions and are isolated in the rear facing direction. Testing of these factors will be done by introducing intentional acoustic noise in the same general frequency range as well as commanding a range finding for two sensors in close proximity.

2.4 Applications of Ultrasonic Sensors

Ultrasonic sensors, though not the most accurate, most precise, nor longest ranging sensors, have found many uses in liquid level detection, presence detection, and robotic sensing. The appeal of ultrasonic sensors is their lightweight, low cost, and low power consumption. Consistent, precise, and accurate object detection for collision avoidance and path planning is an integral part of ensuring safety in the Advanced Air Mobility campaign. Ultrasonic sensors are an easy, reliable way to complete that task. For the DroneMSP application, there will be four ultrasonic sensors mounted on the pallet facing down towards the ground. The sensors main task will be measuring the distance to the ground for landing the aerial vehicle. The secondary task for the sensors is identifying objects below the pallet that may cause a collision. These tasks drove the test conditions for the sensor behavior including incidence angle, operating temperatures varying materials, etc.

2.5 Sensor Characterization Test Process

Sensor characterization is a process in which measurements are taken in a controlled environment. The general process for characterizing a sensor involves determining the physical

quantity to be measured, knowing how the sensor will output data, and collecting truth data for comparing to sensor measurements. Recording a significant amount of measurement data allows one to build a distribution of the output. One important aspect of sensor characterization is approximating that distribution into a probability model that can be used to predict future behavior based on the state and environment of the sensor. As the complexity of testing increases, it becomes more difficult to attribute errors to specific sources because of the number of variables one must consider. Therefore, the characterization process is done using an incremental approach of test build up. The test approach taken is shown in Figure 2.2. This project covers testing with the stationary sensor and target both inside and outside.

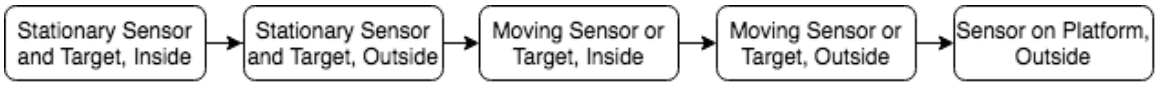

Figure 2.2 Incremental Test Approach Diagram

The incremental test approach has phases where the first phases are simpler so that the factors that affect the sensor measurements can be more easily identified. The last phases are when more realistic conditions are added to the test environment with the final test goal is to collect data for the integrated sensor pallet in flight.

2.6 Project Objectives

The main objective of this paper is performance characterization of range finding sensors. A list of sub-objectives was assembled to construct a path towards completing the main objective. The sub-objectives are:

- Collect range finding data for a variety of test conditions.
- Analyze sensor behavior in the presence external factors that are known to induce errors
- Identify a noise reduction method and implement or simulate it on sensor data.

The main and sub-objectives were completed successfully.

Chapter 3: Literature Review

Performance characterization of sensors takes a methodical test approach and a rigorous understanding of the methods the devices use to perform their sensing. Therefore, a study of the literature involving ultrasonic, lidar, and radar system theory was imperative to analyzing the sensor behavior. Additionally, the methods for statistically modeling sensor behavior was explored so that the models can be applied to the future work of creating a picture of the aerial vehicle's surrounding. Filtering methods were researched including using Kalman filters to reduce the effect of noise and fuse the inputs of multiple sensors.

The fundamentals of ultrasonic range finding physics were given in [17] which enabled exploration of different range finding designs and the methods used to analyze them. It is described in [15] how the design of the ultrasonic sensor affects its performance including its operating frequency, beam spread pattern, and calibration temperature. Researching sensors for navigation applications in different environmental conditions shown in [9] was a pivotal point to begin performance characterization because they described the importance of sensor orientation being consistent between experimentation and application. Once in the operating environment, a list of considerations outlined by Liao et al. [10] in their discussion of factors that affect performance were useful in determining how to build a probabilistic ultrasonic sensor model. The model proposed by Thrun et. al [18] describing the different types of possible measurements was closely correlated with the actual results and was most often cited for other similar experiments.

Making accuracy adjustments after the general performance evaluation procedure was outlined by Gontean et al [7]. The baseline ranging accuracy improvements were simple and straightforward with their piecewise linear regression. Several filters and methods to process data

were given by Taghipour in [20]. Similar filters such as the moving average and median filters were applied for this project to observe any consistencies or deviations from their results. The Kalman filter has been implemented in many applications both for industry and academic purposes. The core concept for a simple 1D Kalman filter that filters while in a constant state was adapted from Tahtawi's [11] work. Tahtawi's work illuminated the need to incorporate a tuning process for the Kalman filter parameters by testing the filter with large and random range changes. The use of a Kalman filter with an ultrasonic sensor was also explored by Zhao et.al [8]. Their work was reviewed for other ways to implement the Kalman filter and its variations. Ultrasonic sensors were able to complement other positioning sensors in the suite by providing calibration during drift. The research presented in [8] was utilized to ensure there was emphasis on range finding accuracy tests at higher sampling rates which provide data fast enough for what will be required in flight.

Chapter 4: Data Collection, Analysis, and Modeling

4.1 Test Setup

The MB-1242 ultrasonic sensor uses the inter-integrated circuit (I2C) serial communication protocol laid out in [1]. For testing, the sensor was connected to the 3.3V pin for low power consumption with the serial data and serial clock line going to the I2C pins on the Raspberry Pi. A majority of sensor measurements were taken with only one sensor connected and commanding range measurements. Two sensors were connected in parallel as shown in the general wiring diagram in Figure 4.1 for observing crosstalk errors.

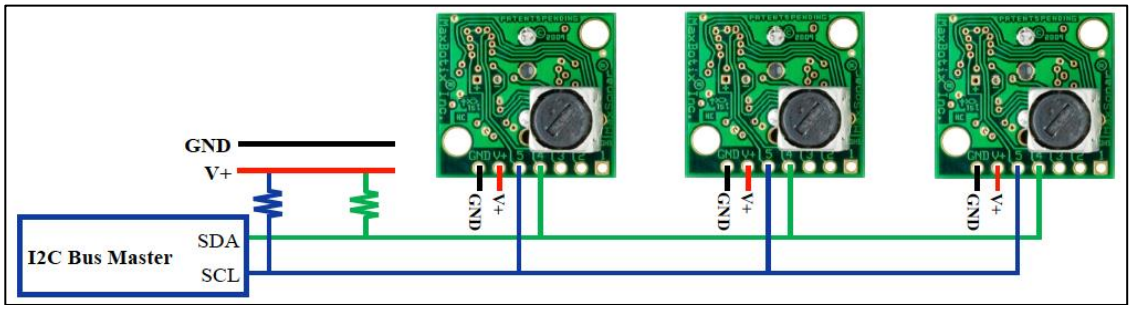

Figure 4.1 MB-1242 Wiring Diagram (MaxBotix, [3])

Several limitations existed in characterizing the sensor. COVID-19 prevented testing the sensor in a dedicated lab. Testing was executed in a family residence which introduced several noise sources including error from low precision measurement methods and a noisy "noise free" environment e.g. reflective surface clutter, audio noise, uncontrolled fluctuation in temperatures and humidity, etc. These factors are considered in the data analysis. The test setup for most of the range finding measurements is shown in the Figure 4.2 A 8"x8", ¾" plywood sheet was used as a target and mounted off of an arm to separate it from the base and reduce clutter. The sensor was fixed to the base and the base was fixed to the ground while the target was manually moved backwards. The only variation from this setup was the material of the target being swapped out

for the material tests and a larger 40”x24” plywood board utilized for the maximum range and temperature tests when the range was increased to ~300 to ~500cm.

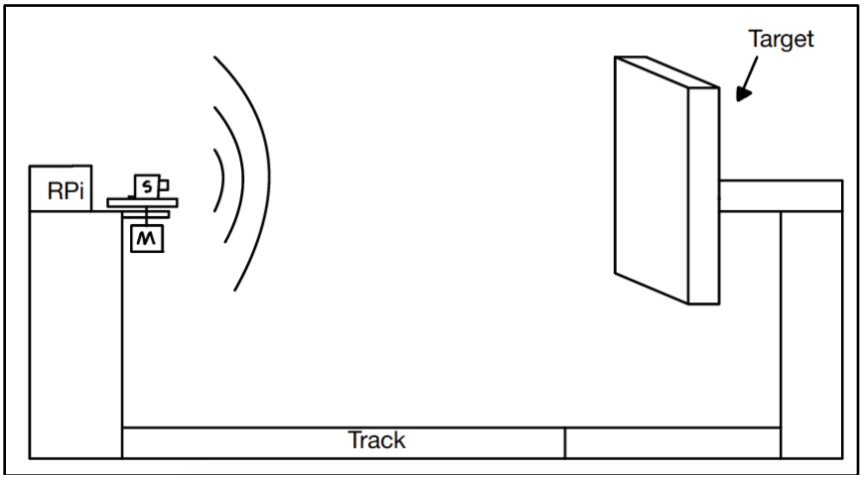

Figure 4.2 Range Test Setup

The ultrasonic sensor was positioned and leveled to aim at the middle of the plywood sheet. It was mounted onto a NEMA 17 stepper motor which operates at 200 steps/revolution i.e. 1.8°/step. The motor was used to rotate the sensor in 1.8° increments off center for the field-of-view testing since the sensor pallet will have ultrasonic sensors angled to do object detection to the side. The field-of-view test setup is shown in Figure 4.3.

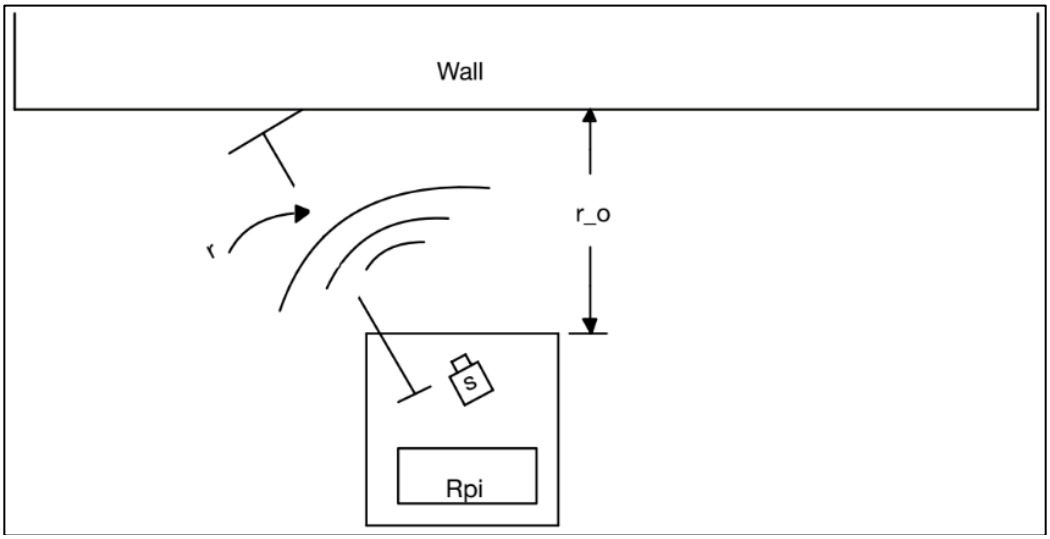

Figure 4.3 Field-of-View Test Setup

4.2 Test Conditions and Configurations

Exhaustive sensor characterization would require infinite test conditions for every change in parameters that affect the sensor measurements. A test condition table shown in Table 4.1 was used to compile of all the different test configurations and conditions to limit the scope of the testing based on time and resource constraints as well as focus on the sensor pallet use case. The explicit details of each specific test condition were listed in the corresponding subsection. A "noise free' environment was the first data collection to define the base setup. The noise free setup had the sensor indoors at a 0° angle from boresight and with zero "clutter" in the relative area of the target.

Table 4.1 Test Conditions and Configurations

Sensor Configuration (# of sensors)	Specific Test Conditions	Ranges (cm)
Baseline	none	40 to 260, 20cm increment
Maximum Range	Increased Target size of 40"x24"	500
Field-of-View	Angle of Incidence Varied from 0° to ±23.4°	50, 100, 150, 200
Material	Plywood, Asphalt, and Concrete Target	40 to 260, 20cm increment
Temperature	Cold: 47°F, Room: 70°F, Hot: 115°F	40 to 260, 20cm increment
Vibrations	60Hz Applied to Sensor Housing	40 to 260, 20cm increment
External Interference (2)	none	40 to 260, 20cm increment

Sensor characterization for other range finding sensors with access to a laboratory and high precision instrumentation should observe other characteristics of the sensor behavior. More specific test conditions could include changing humidity, moving targets, and intentional acoustic noise.

4.3 Collection and Analysis

The next subsections are the compilation of all the data that was collected to characterize the performance of the MB-1242 ultrasonic sensor. The subsections are delineated by the internal or external effect that they had on the sensor.

4.3.1 Baseline Range Accuracy

The first step to characterizing the sensor was to baseline its precision and accuracy with the simplest test setup. After measuring with the obstacle (target) as shown in Figure 4.2, the estimated distance using the ultrasonic sensor was compared to the actual distance to generate a range error. The sensor was programmed to measure a cluster of measurements every 100ms. The range error for all distances is shown in Fig 4.4. A positive error indicates that the sensor estimated further than the actual distance i.e. sensor reports 101cm when true distance is 100cm.

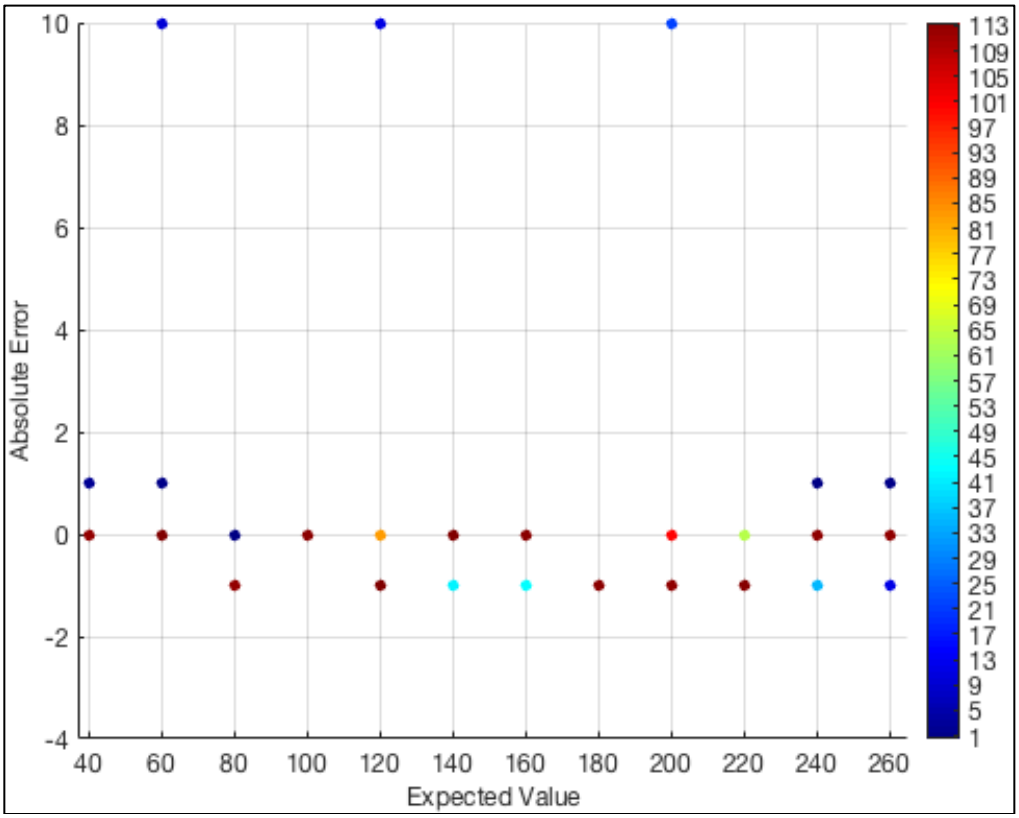

Figure 4.4 Range Error, All Ranges

As expected, the ultrasonic sensor was quite accurate with the largest error from a non-missed measurement being 1cm where missed measurements are readings of the maximum range at 765cm. It should be noted that the resolution of the sensor was 1cm. Therefore, errors less than that could not be discerned. However, for the application on the sensor pallet, the 1cm resolution was sufficient.

4.3.2 Maximum Range Noise Model

The first task in developing the sensor model is finding the probability of a range measurement given the actual range. The sensor model can be built using an approximation of raw sensor data. Building the model using sensor data requires one to take many measurements at a fixed distance. Figure 4.5 below shows 2000 measurements for a fixed range of 500cm.

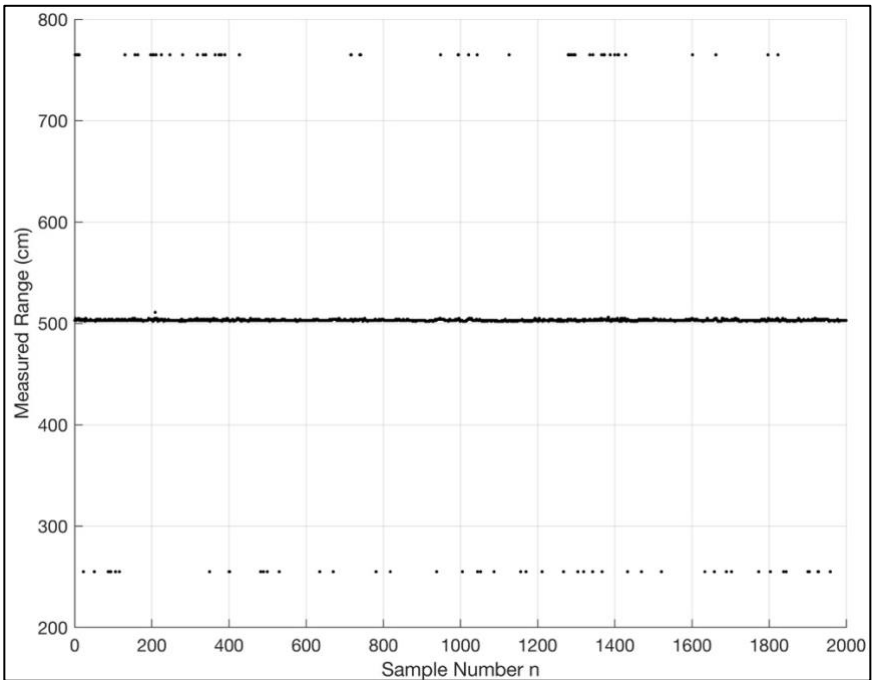

Figure 4.5 Maximum Range Measurements

A distribution of range measurements was accumulated to build the histogram in Figure 4.6. Occasional range reports of the target were missed. This occurrence caused random reporting of 765cm and 255cm. The histogram appears to be multi-modal as a result.

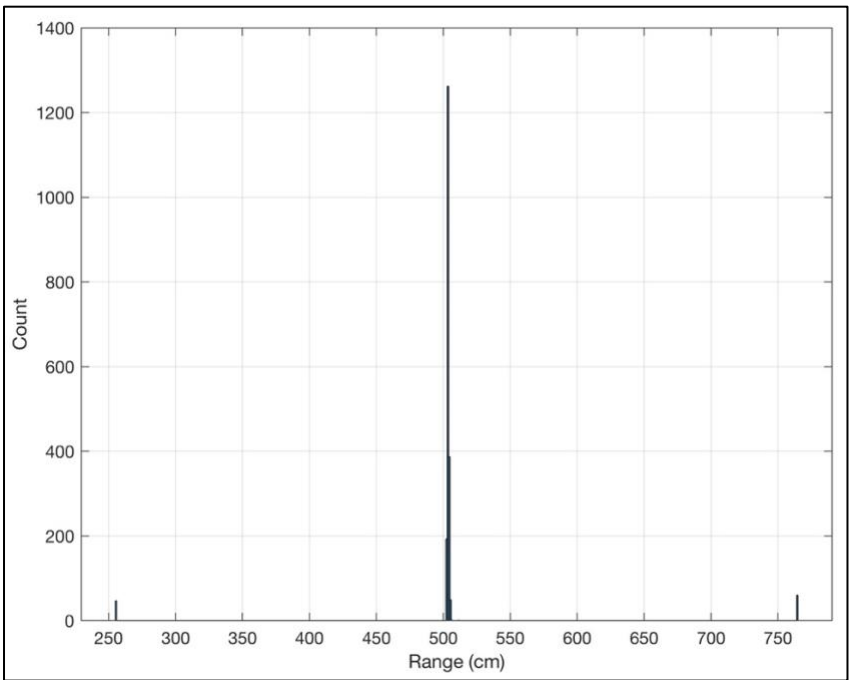

Figure 4.6 Maximum Range Histogram

Sporadic 765cm and 255cm range measurements can easily be filtered out with a simple time domain filter or fusion from other range finding inputs. After filtering those out, a new scatter plot and histogram were generated in Figures 4.7 and 4.8, respectively.

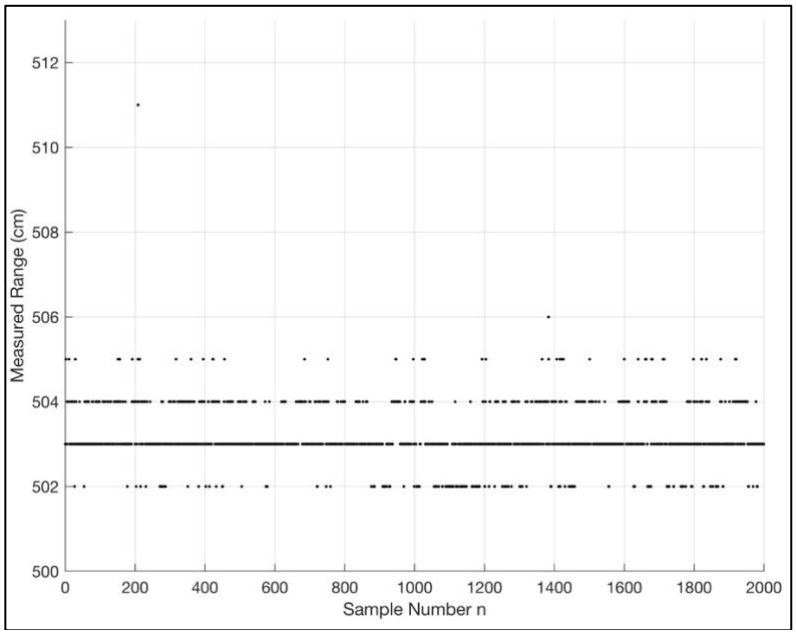

Figure 4.7 Maximum Range Measurements, Masking Missed Reports

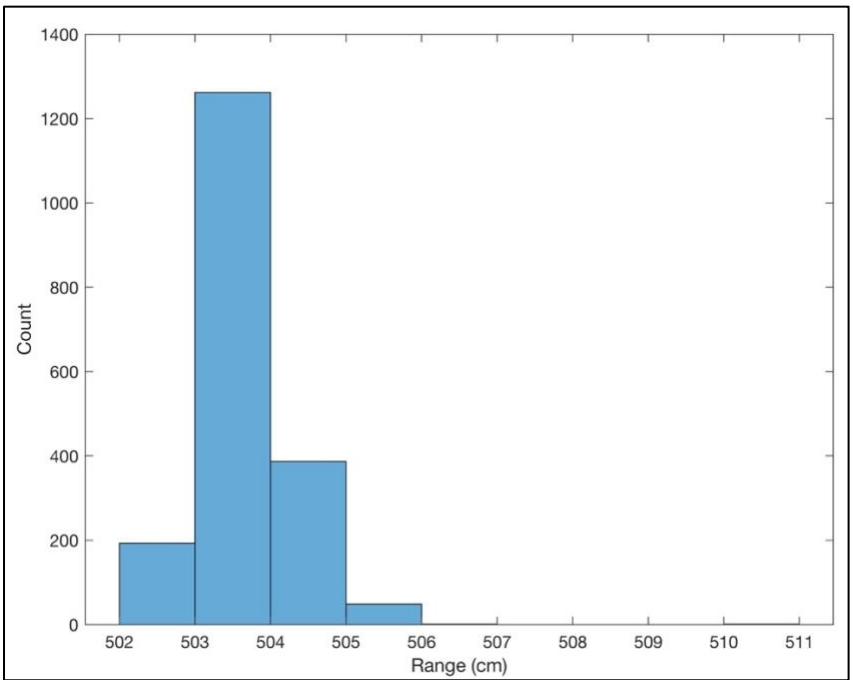

Figure 4.8 Maximum Range Histogram, Masking Missed Reports

These figures more accurately demonstrate the effect of gaussian noise on the sensor. A majority of measurements in Figure 4.7 appear close to the actual range. Additionally, the histogram shows a single peak around 503cm.

4.3.3 Field-of-View

The ultrasonic sensors will be mounted on the pallet so that they are pointed at the ground. The sensors may be at a slight angle while flying that prevents them from being perfectly orthogonal with the landing surface. Additionally, an intentional angling of the sensor away from the centroid of the pallet helps to prevent cross talk and accomplish its second goal of mid-air object detection, tracking, and avoidance. A large incidence angle reduces the amount of energy reflected away from the sensor which affects the range reporting. The sensor field-of-view is then required to determine the operational area in which the sensor receives enough energy to report an accurate range. The simple test setup where the sensor was swept back and forth in 1.8° increments as shown in Figure 4.3. was used to find the breakaway point i.e. the angle at which

the sensor no longer reports the radial range. As the sensor is angled away from the wall, the radial distance (line-of-sight line from the sensor to the wall) increases. The radial distance, r, can be described by the equation below where the r_o is the orthogonal distance to the wall.

$$r = \frac{r_o}{\cos(\theta)} \tag{8}$$

Figure 4.9 shows the field-of-view for the sensor at a distance of 50 cm to the closest point on the wall. The sensor breakaway point at 50cm was determined to be ~23° and was set as the largest angle needed for other field-of-view tests. The field-of-view for the distances of 100cm, 150cm, and 200cm are shown in Figures 4.10, 4.11, and 4.12 respectively.

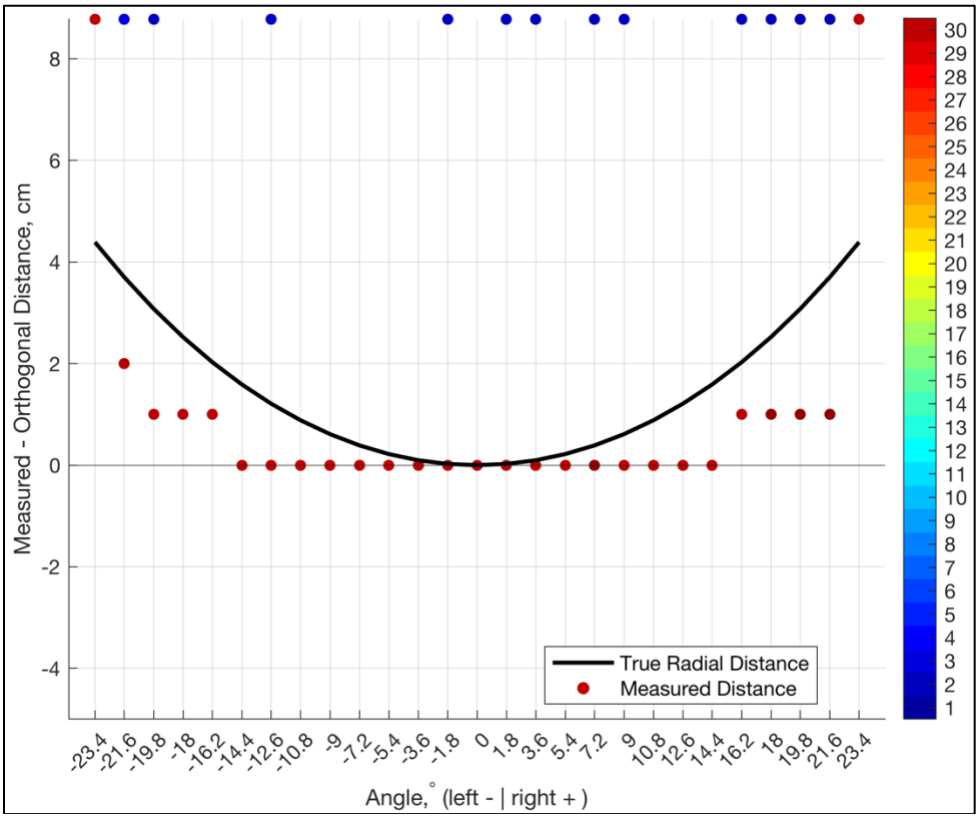

Figure 4.9 Field-of-view, 50cm

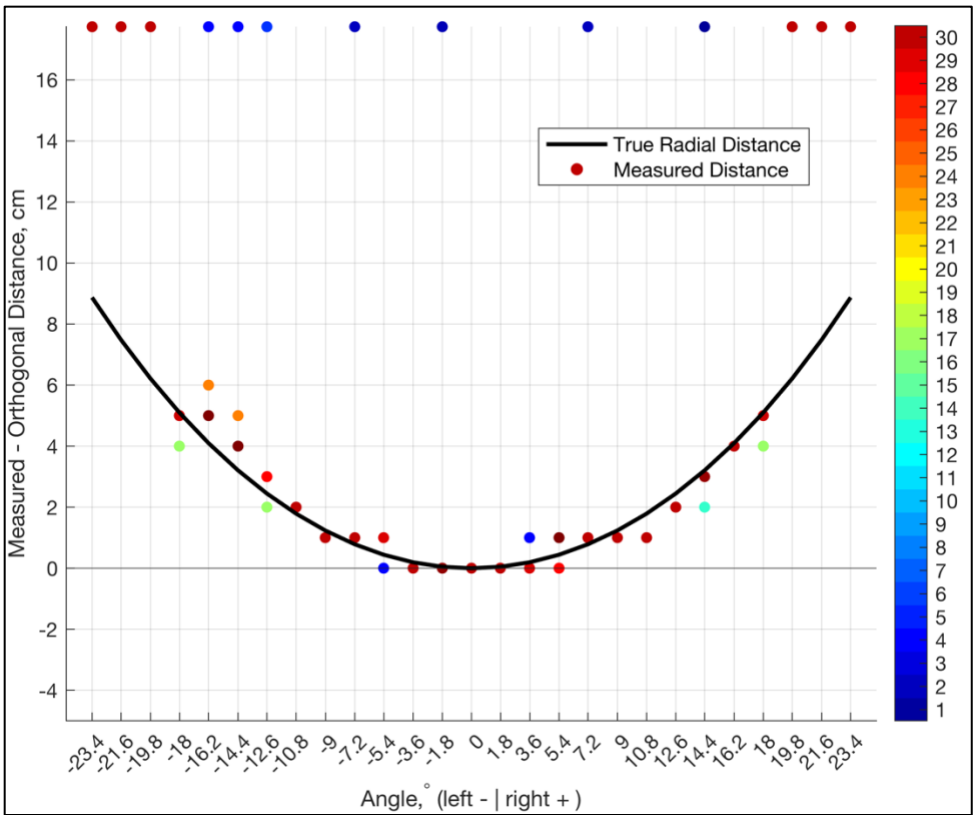

Figure 4.10 Field-of-view, 100cm

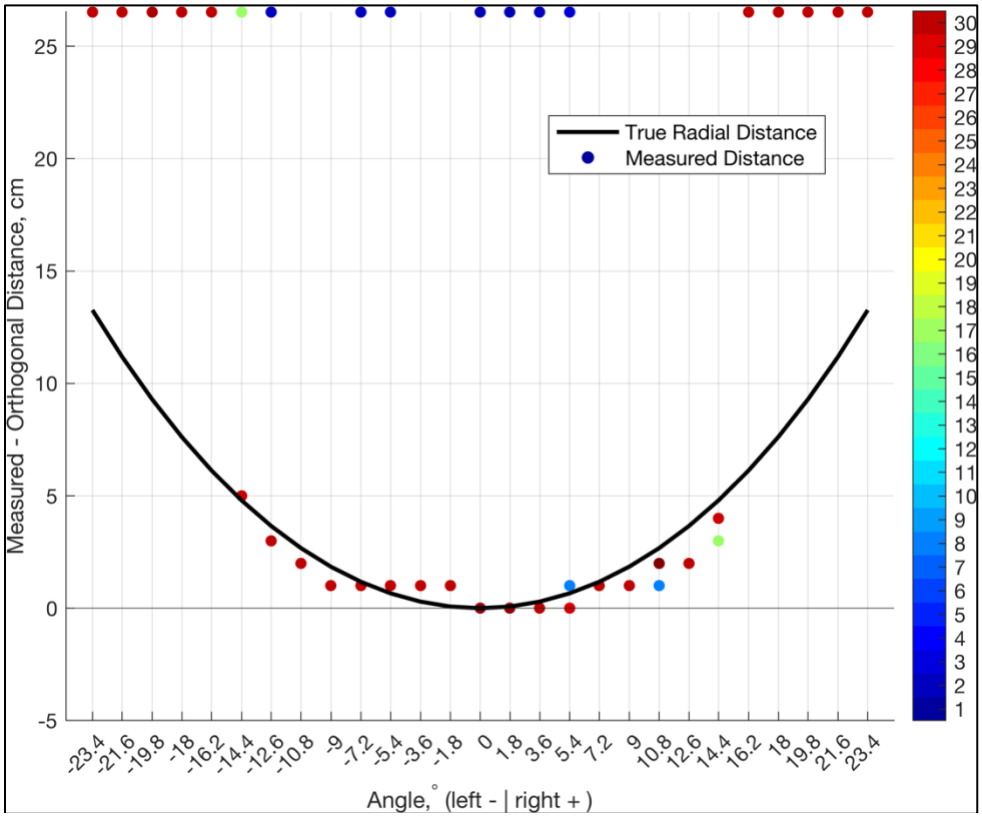

Figure 4.11 Field-of-view, 150cm

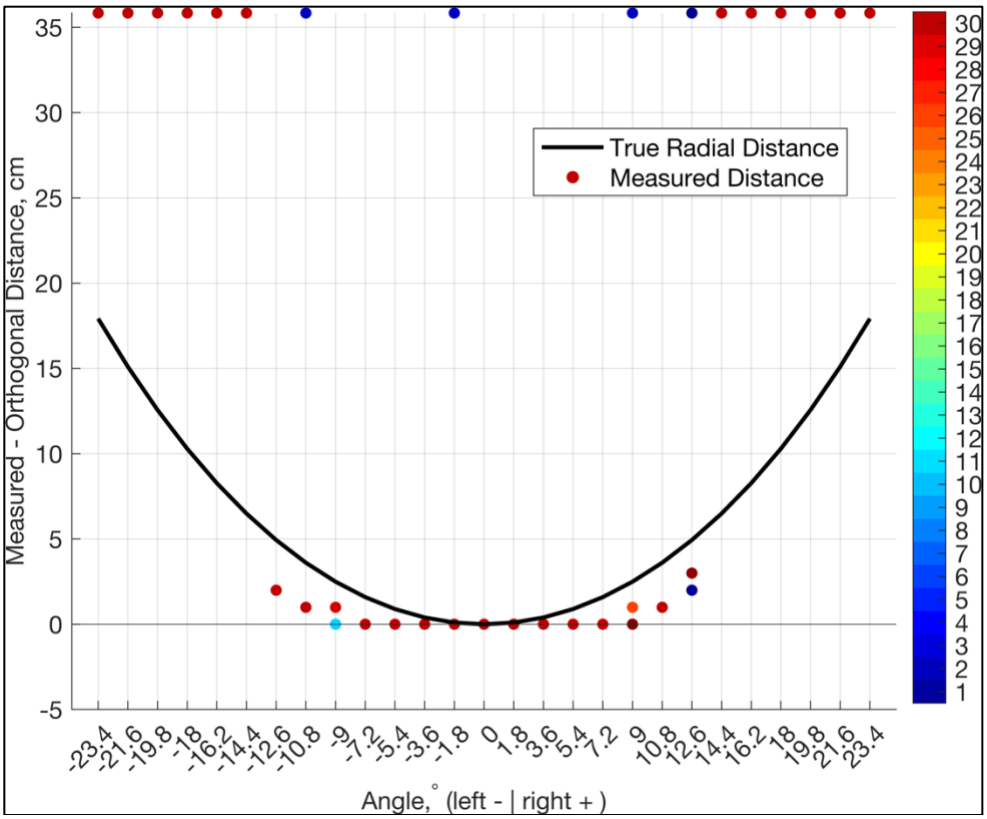

Figure 4.12 Field-of-view, 200cm

The largest angle of incidence in which reliable range measurements are reported are 23.4° for 50cm, 18° for 100cm, 14.4° for 150cm, and 12.6° for 200cm. Less ultrasonic energy reaches the sensor as the range increases lowering the chance of hitting the intensity threshold which results in smaller angles that define the field-of-view.

4.3.4 Material

The aerial vehicles for the DroneMSP may have to land on any type of terrain. Several materials were tested to ensure that the US could provide accurate ranging regardless of the material it was detecting. Research on the acoustic absorption coefficients of wood, concrete, and asphalt showed that they are similar. The shorter ranges of testing also meant the effects of the different acoustic absorption coefficients would be undiscernible as evidenced in Figure 4.13, 4.14, and 4.15.

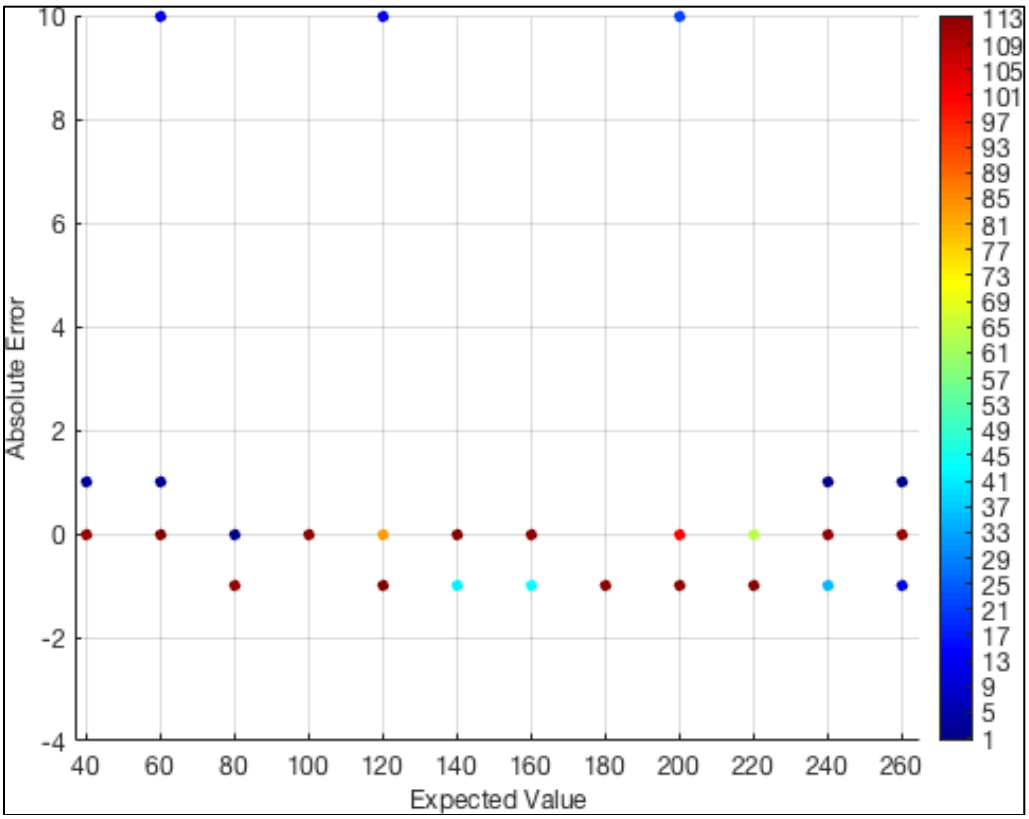

Figure 4.13 Range Error, Plywood Target

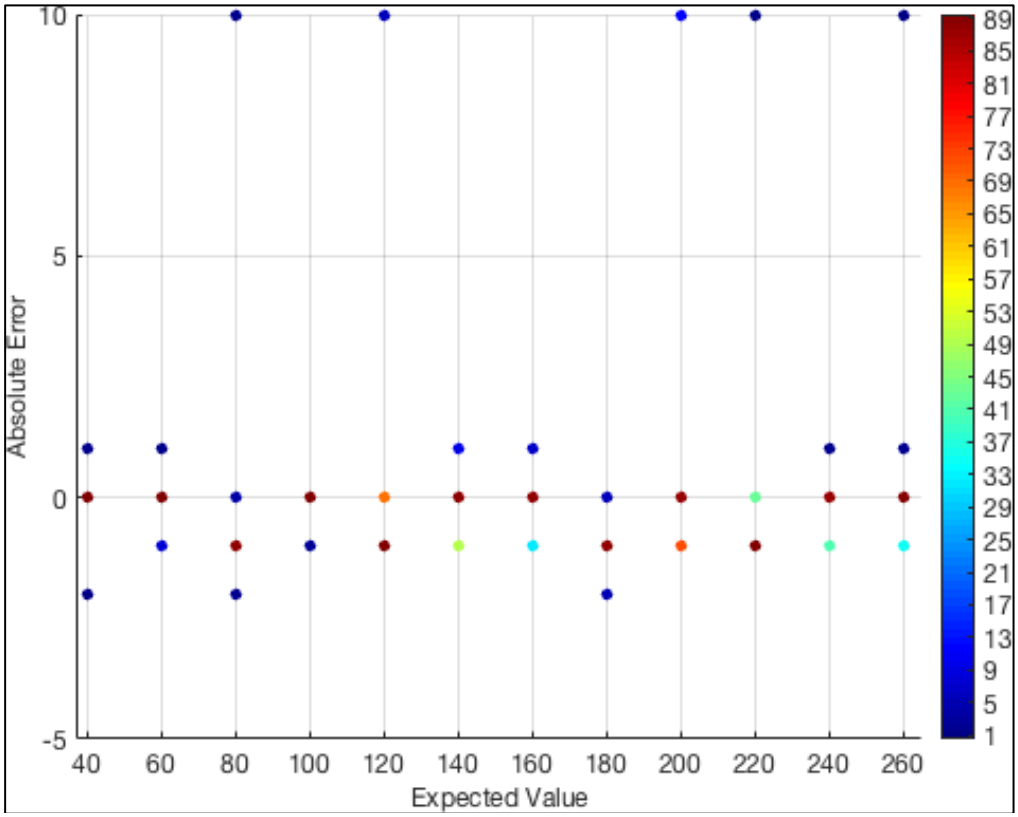

Figure 4.14 Range Error, Asphalt Target

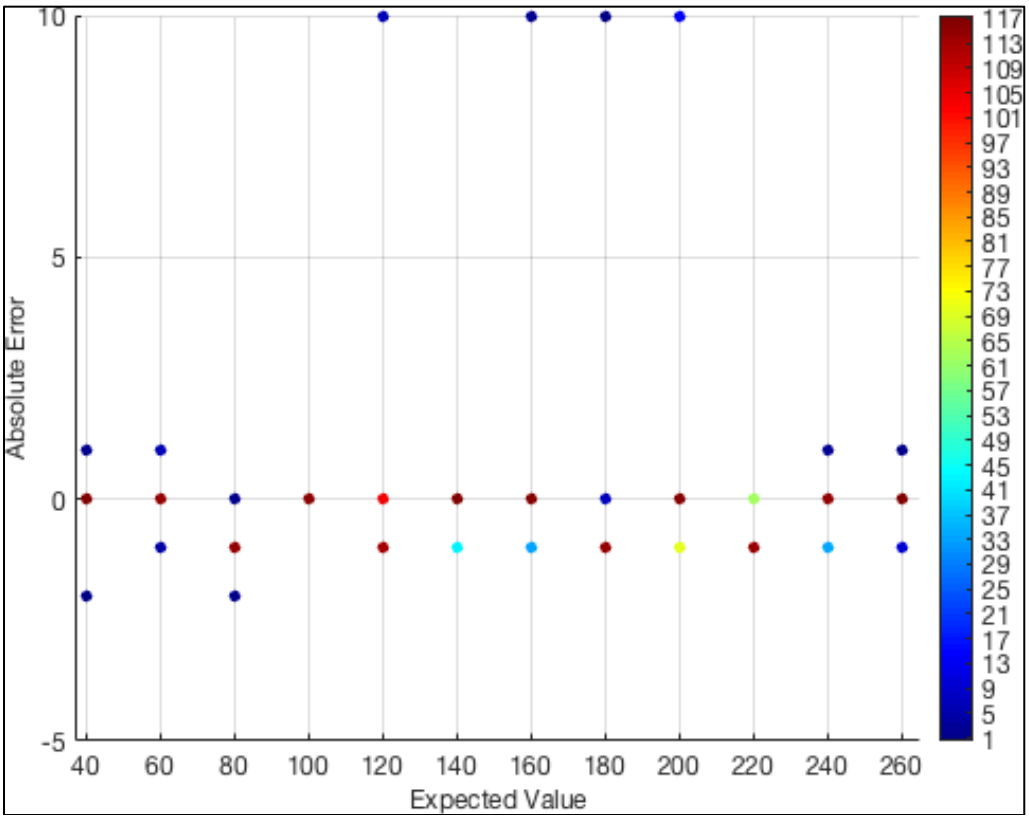

Figure 4.15 Range Error, Concrete Target

Future research could analyze the maximum detection range for a set target size given varying target materials. Additionally, material testing should include range accuracy when sensing more naturally occurring landing areas such as grass and dirt plots.

4.3.5 Temperature

The accuracy of the ultrasonic sensor, as discussed in Chapter 2, is dependent on many environmental factors including temperature. The lack of a precise temperature measuring device and limited control on the temperature through the entire testing area forced this testing to be split into three subjective categories: sensing in cold, room, and hot temperatures. Cold was classified as 47°, room was classified as 70°, and hot was classified as 115°. A semi-enclosed box was built to encompass the sensor while measuring range. Air, both hot and cold, was forced through a vent and a temperature measurement device within the enclosure measured the

temperature. It was already known that the sensors used did not compensate for temperature changes, therefore, discernible errors were expected. The range error at room temperature is shown in Figure 4.16.

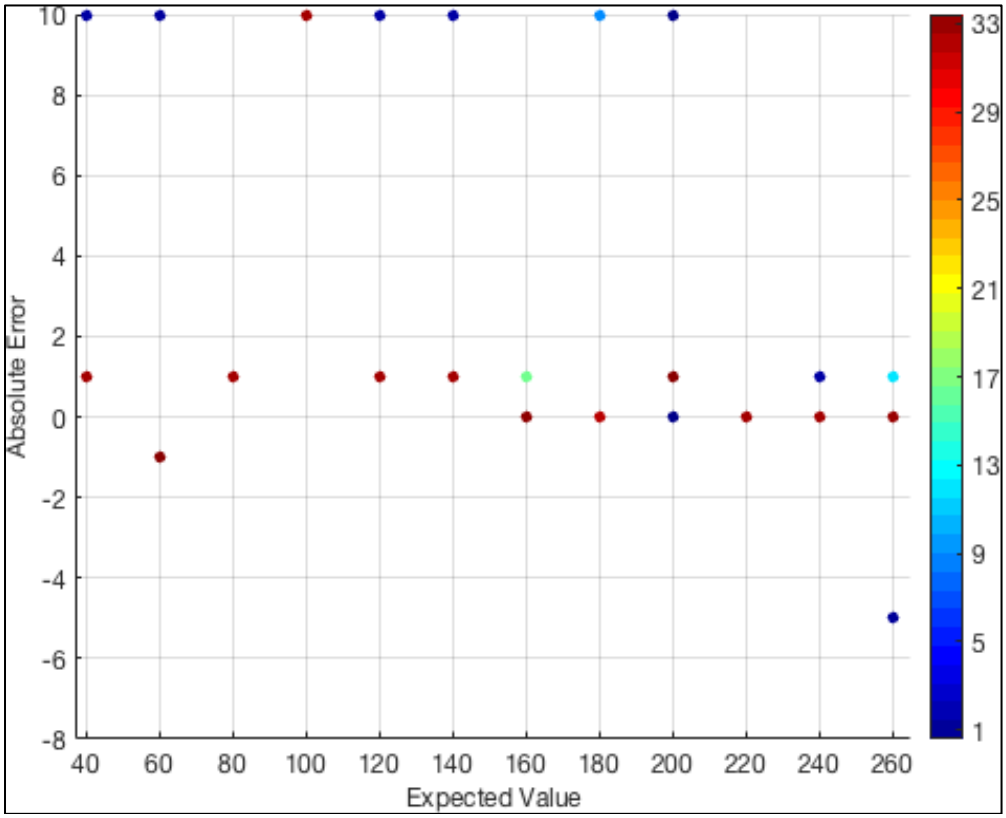

Figure 4.16 Range Error, Room Temperature

The difference from the calibrated temperature of 68°F in the sensing area was expected to change the wave propagation speed and induce measurement errors. Converting the 115°F temperature into Rankine and plugging into (7) yields a 30% difference between the true and measured range. One can see in the Figure 4.17 that the actual range error results were on the order of 1-2cm.

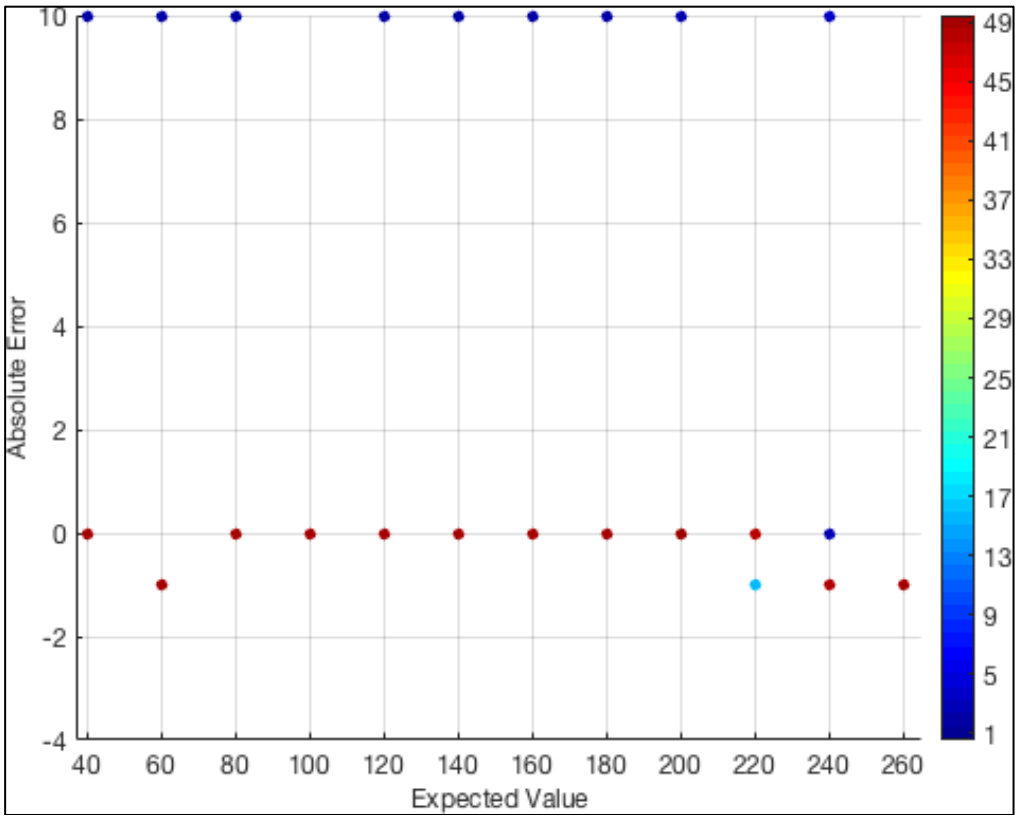

Figure 4.17 Range Error, Hot Temperature

The reason for the minimal error was a gradient of temperatures in the ranging area. The temperature enclosed in the box was 115° but the target was 10s of centimeters away. Therefore, a gradient going from 115° to room temperature at 71° would mean less variance in the wave propagation speed from room temperature and reduced sensing errors. The same temperature gradient occurred for the “cold” sensing except this time the temperature increased as it got closer to the target. It was expected that the sensor would report larger estimated ranges since the wave propagation speed decreased. This can be seen in Figure 4.18.

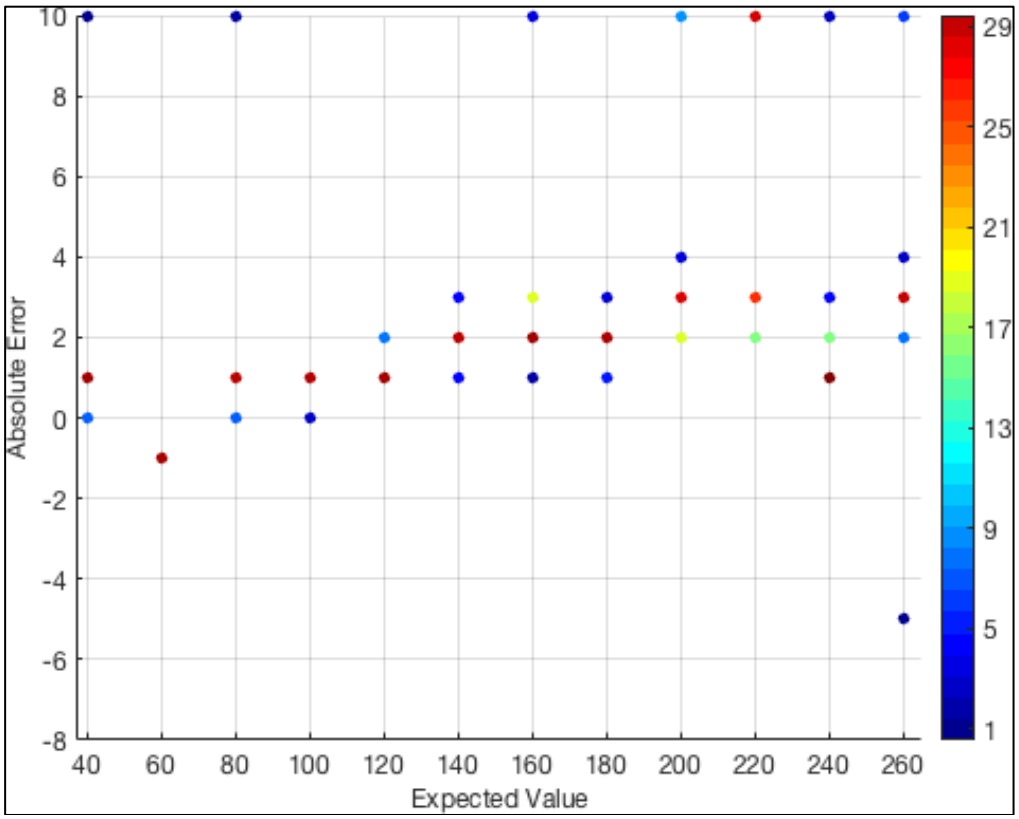

Figure 4.18 Range Error, Cold Temperature

4.3.6 Vibrations

The sound pulses from the ultrasonic range finder are at a frequency of 40kHz. It would be anticipated that flying an aerial vehicle with rotors such as a quadcopter would vibrate at frequencies at or near that transmit tone. The operation of these sensors on those vehicles would have impacts of that noise on range finding accuracy. A test was completed where the sensor would take measurements while vibrating at 60Hz. One can see in Figure 4.19 that the accuracy compared to the baseline is effectively the same.

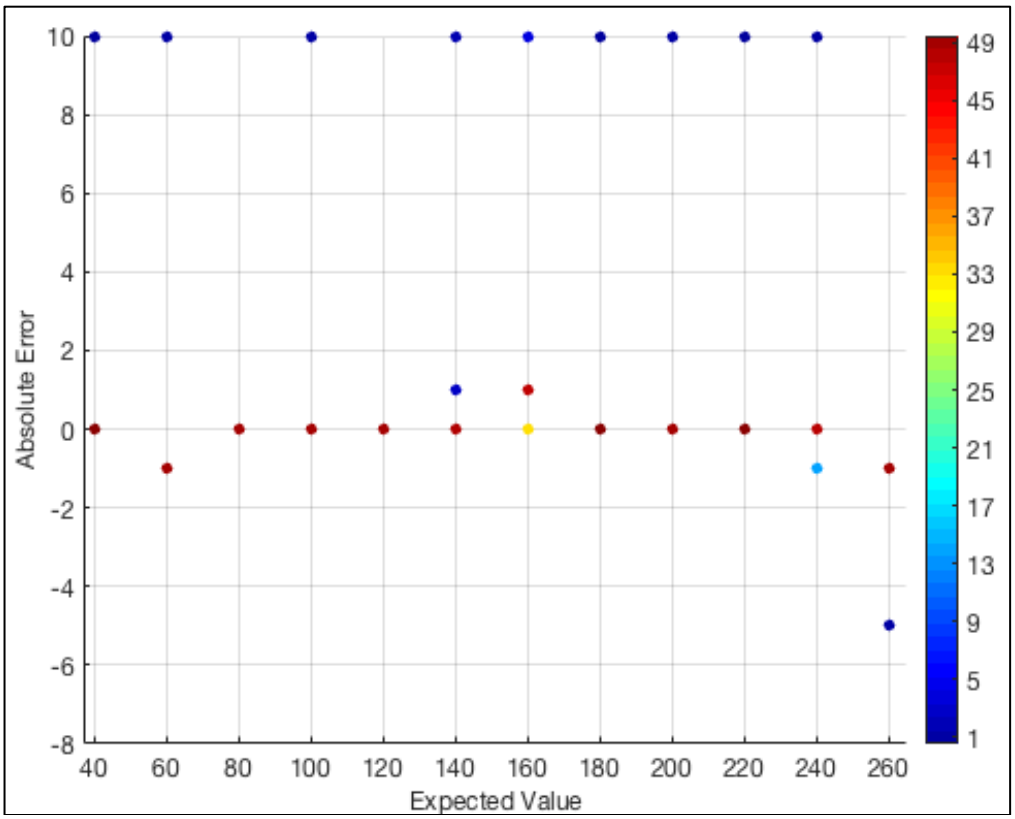

Figure 4.19 Range Error, 60 Hz Vibration Noise

With limited frequency control of the vibration noise, the vibrations had minimal impact on the ranging accuracy. Even the harmonic frequencies of the vibrations would not be near the frequency of the pulses used to make ranging measurements. Future work in a lab or flight test setting should examine the effect of vibrations of the aerial vehicle during flight on the accuracy of the range finders.

4.3.7 Internal Interference

Crosstalk between two ultrasonic sensors can occur when the sensors are transmitting at the same frequency simultaneously. Two sensors were positioned 6” apart and pointed at the same plywood target. The first test scenario had both sensors command range readings without regard to the other sensor. The expectation was that the ultrasonic pressure waves would be received by both sensors and the small difference in transmission timing would induce errors. The second

scenario had sensors wait for the other sensor to complete the ranging cycle before command a range reading. The expectation was that no range errors would be evident as the sensors would no longer receive ultrasonic energy from the other transmitter. The range error results for each sensor in the first scenario are shown in Figure 4.20.

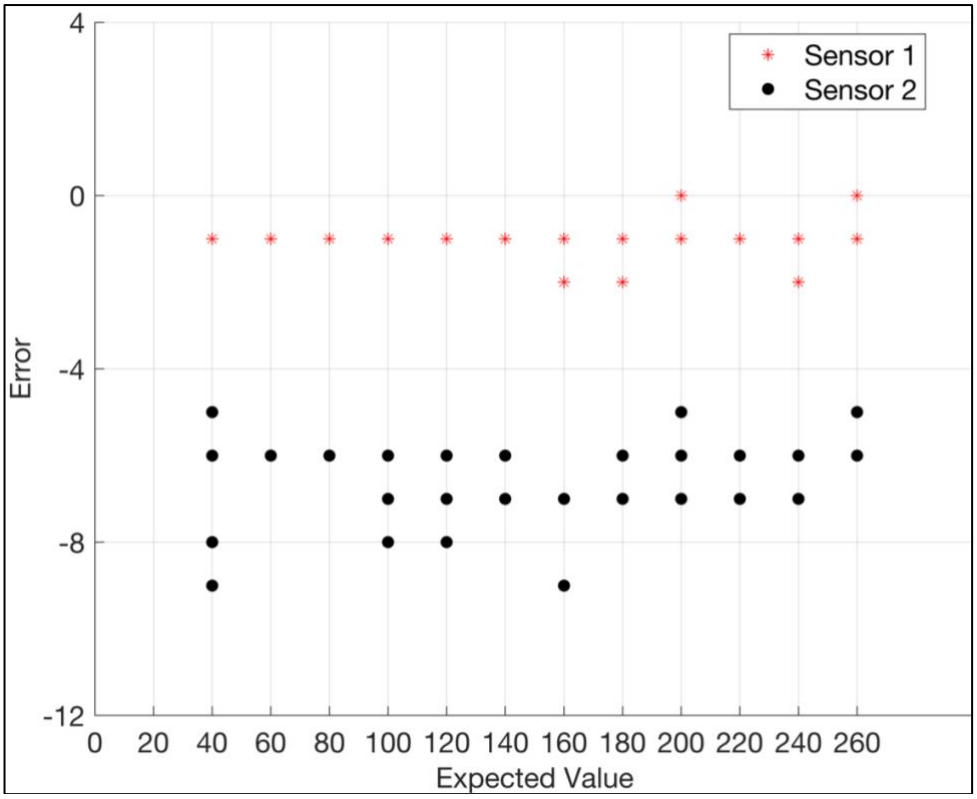

Figure 4.20 Range Error, 2 Sensors Simultaneous Transmission

The sensor 2 range readings occurred shortly after sensor 1 even though they were commanded at the "same time." The small processing and circuit delays prevented exactly simultaneous transmission. This is evident by the sensor 2 readings reporting a shorter range since they likely received the transmission of sensor 1. The range error results for each sensor in the second scenario are shown in Figure 4.21. One can see that the crosstalk induced errors were reduced using the sequential transmission method.

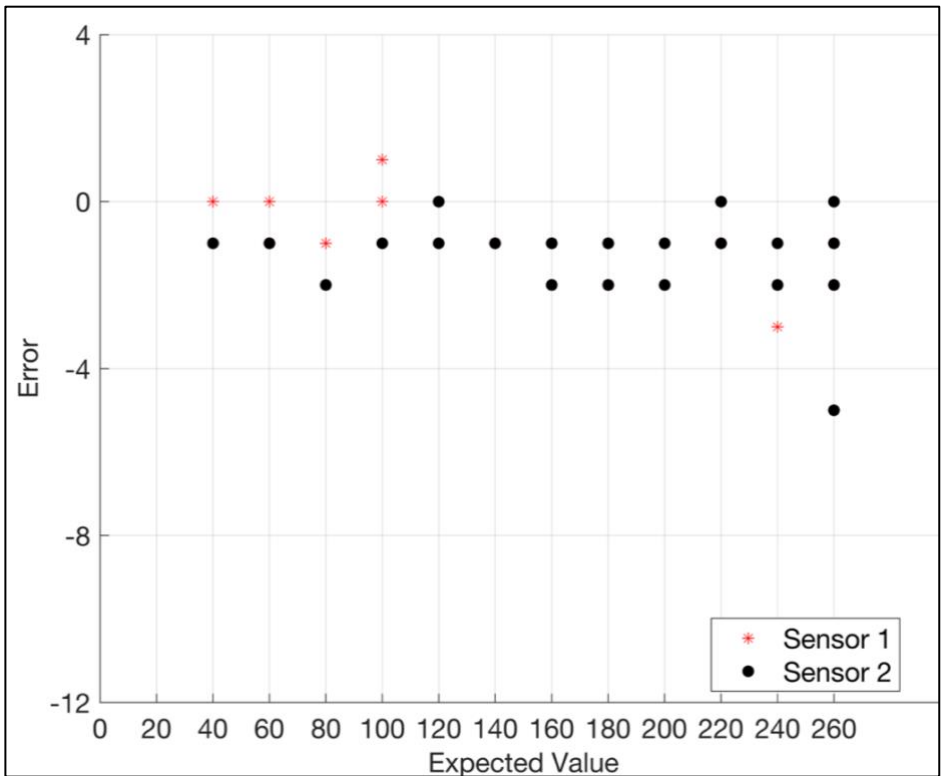

Figure 4.21 Range Error, 2 Sensors Sequential Transmission

The tradeoff of sequential transmission is that the number of range updates the sensor pallet receives decreases since increasing the number of sensors increases the time between each sensor individual range reading.

4.3.8 External Interference

Interference from the aforementioned ultrasonic noise producers can be quantified if the noise levels of those producers are known or can be measured. Testing was completed inside and outside with potential ultrasonic noise present. It was inconclusive on whether any measurement errors were due to external ultrasonic transmitters. This is due to the limitations of the home test setup and limited equipment where the external interference could not be measured. Future work should include experiments in an isolated environment such as an anechoic chamber with only the sensor and the ultrasonic noise producers to determine the frequency and magnitude of the errors produced.

Chapter 5: Noise Reduction Results

5.1 Temperature Compensation

Improvements in ranging accuracy can be achieved by accounting for the various known factors that affect the sensor. The first simple improvement is compensating for the temperature of the medium of which the wave propagates through. Implementing the compensation coefficient in (7) was expected to reduce the error. The changes in speed of sound are more evident over longer ranges, therefore, the range was increased and the target size was enlarged to ensure consistent detections. Figure 5.1 and Figure 5.2 show the ranging errors when not compensating and compensating in the calculation.

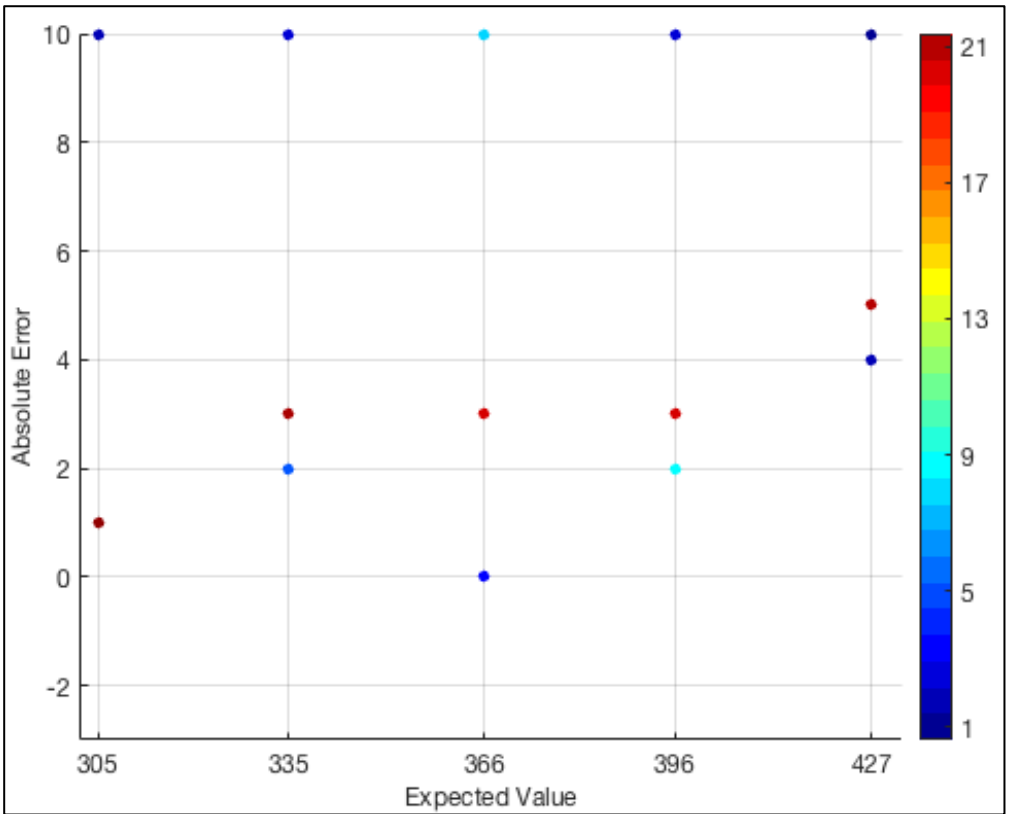

Figure 5.1 Temperature Uncompensated Ranging

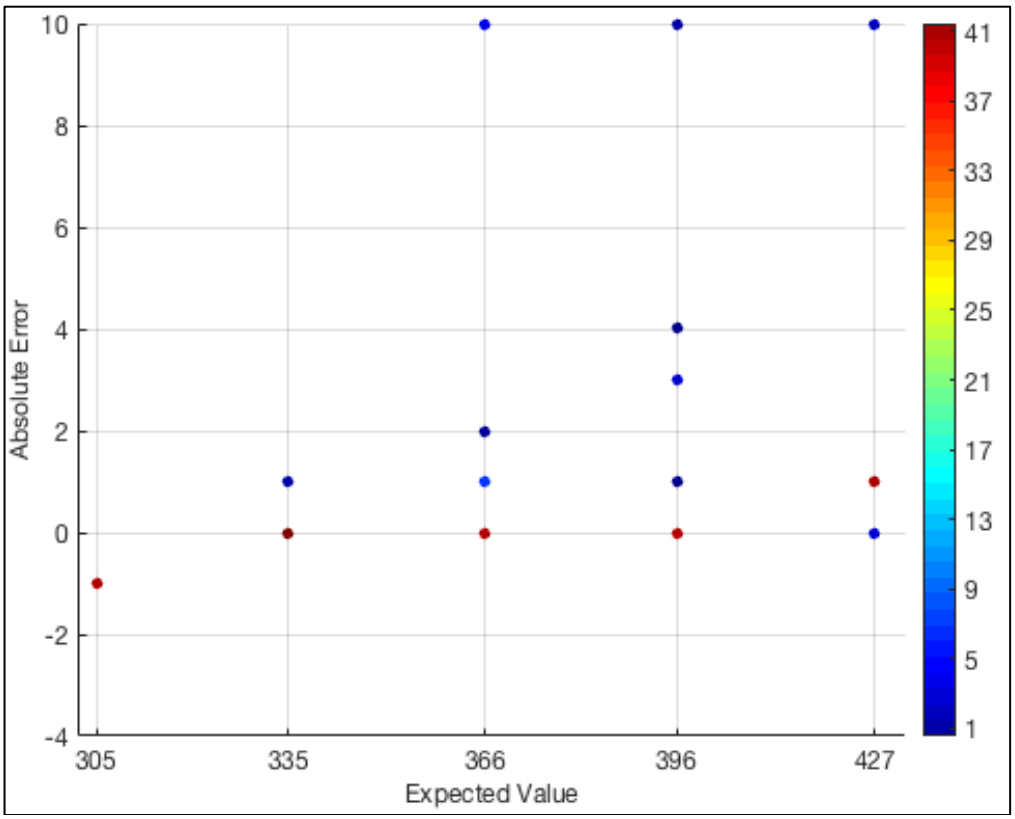

Figure 5.2 Temperature Compensated Ranging

It was immediately obvious that implementing temperature compensation was effective during the experiment by the majority of measurements that were shifted to be the correct range. The short-range use for landing and large obstacle detection implies that errors induced by low or high temperatures should not be as significant. However, one can see in Table 5.1 that compensating the range measurements reduced the average ranging error significantly.

Table 5.1 Temperature Compensation Range Error Results

Range (cm)	Average Range Error (cm)	
	Uncompensated	Compensated
305	1.00	1.00
335	2.821	0.067
366	2.739	0.196
396	2.724	0.447
427	4.931	0.921

As alluded to previously, the assumption that the temperature around the sensor pallet is exactly the same as the temperature of the area in which the ultrasonic wave travels through can cause problems. The temperature gradient over the range for which this sensor will normally operate should not cause significant errors as the sensors max detection range is ~500cm. This assumption should be considered during implementation.

5.2 Additive Gaussian Noise Filtering Fundamentals and Methods

A process to reduce the error induced by gaussian noise requires several important steps. The source of the noise must first be understood and approximated quantitatively. The next step is to identify which methods are best for the identified noise, including the tradeoffs of each method. The final step is to determine the theoretical results to set an expectation for implementing the noise reduction method. The following subsections outline this process.

5.2.1 Range Sensor Model

Sensor models for autonomous aerial vehicles have already been studied and compiled by Thrun et. al in [18]. The beam based sensor model proposed is a mixed density model used for proximity sensors that accounts for measurements from: known obstacles, unknown obstacles, crosstalk, and missed obstacle detection. Noise is also included in the model due to: measurement uncertainty of known obstacles, position uncertainty of known and unknown obstacles, and random missed measurements.

The measurement noise occurs due to uncertainty in the ranging. It is described by a gaussian distribution which takes the general form in (9).

$$P_{hit}(z|x,m) = \frac{\eta 1}{\sqrt{2\pi b}} e^{-\frac{1(z-z_{\exp})^2}{2b}} \tag{9}$$

The measurement noise is the focus of this section as is it more common than the other forms of noise and many methods exist in filtering it out. Gaussian measurement noise can originate from any of the factors listed in section 2.1.3. The graphical representation of this density function is shown in Figure 5.3.

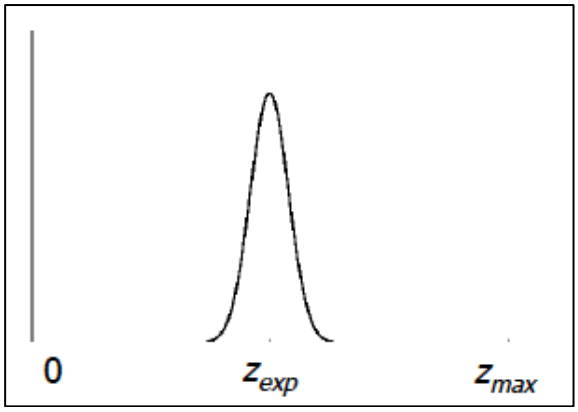

Figure 5.3 Measurement Noise Density (Thrun [18])

Unexpected obstacles can occur in any dynamic environment that the aerial vehicle operates in. Consider two moving obstacles that show up in the viewing field of a ranging sensor: a close personal uav and further away bird. When the uav is present, it is measured. In order to measure the bird, the bird must be present and the uav must be out of the viewing area. This results in measurements that are unexpected, especially at close ranges. The location of unexpected obstacles can be estimated, however, to simplify the problem Thrun et. al. suggests treating those measurements as noise. The unexpected obstacles take the form of an exponential distribution that falls off as the range increases when treated as noise. The general form in (10) describes the probability distribution.

$$P_{unexp}(z|x,m) = \begin{cases} \eta\lambda e^{-\lambda z} & z < z_{exp} \\ 0 & otherwise \end{cases} \quad (10)$$

The graphical representation of this density function is shown in Figure 5.4.

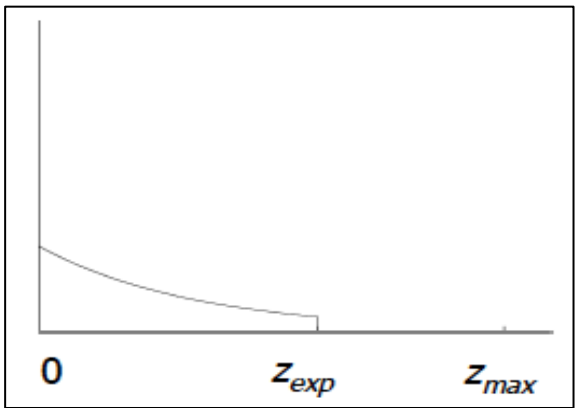

Figure 5.4 Unexpected Obstacles Density (Thrun [18])

An obstacle in front of the sensor can sometimes be missed altogether as is the case of a high noise floor or measurements that reflect completely away as a result of high incidence angles. The result of a missed measurement is the sensor reporting the maximum range. The maximum range reports are then combined into a uniform density function while in reality the measurements are a discrete distribution.

$$P_{max}(z|x,m) = \frac{\eta 1}{z_{small}} \tag{11}$$

The graphical representation of this density function is shown in Figure 5.5.

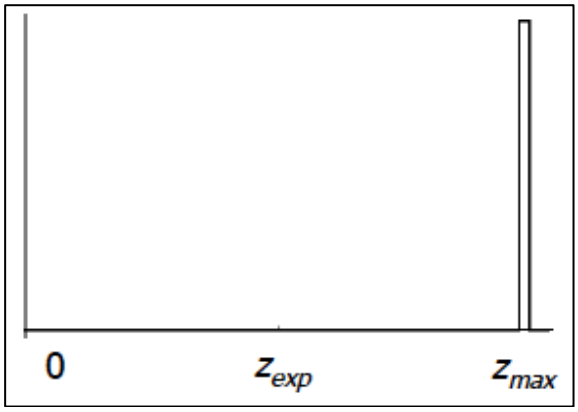

Figure 5.5 Maximum Range Density (Thrun [18])

The internal and external interference in the form of cross talk as well as phantom readings from multipath effects are simplified into a uniform distribution that covers the detection range of the sensor. These can also be any other inexplicable source of noise. The graph in figure 5.6 shows 0

to z_{max} when in reality the sensor minimum may not be 0 such as is the case with the MB-1242 that reports all objects closer than within 20cm as 20cm due to limitations in ultrasonic physics.

$$P_{random}(z|x,m) = \frac{\eta 1}{z_{max}} \tag{12}$$

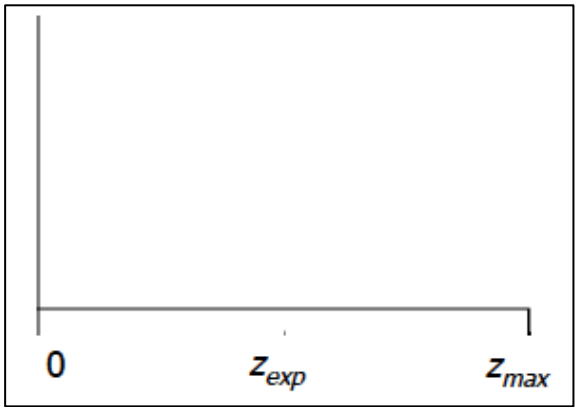

Figure 5.6 Random Measurement Density (Thrun [18])

The intrinsic parameters that describe these densities can be assumed or found using the sensor data. A series of tests were done on different days to collect 20000 measurements at a range of 500cm. The stationary testing and noise free environment meant that a majority of measurements resulted in the sensor reporting the correct range. So, the noise that was expected from the mixed density model was not seen in the basic test. Therefore, this noise was generated in MATLAB and added to the raw sensor measurements to analyze the effectiveness of the noise reduction methods. Most noise filtering methods deal with additive gaussian noise. This paper examines three filters whose goal is to eliminate or reduce the effect of gaussian measurement noise.

5.2.2 Moving Average Filter

The moving average filter is one of the first filters to be tested because of its simplicity and easy implementation. It is described by (13)

$$y[i] = \frac{1}{M}\sum_{j=0}^{M-1} x[i+j] \tag{13}$$

where M is the window size of the filter (i.e. number of points to take in average), i is the current index, and j is the index of all of the other points to be taken in the average. The j indices can either be single sided which are easier to implement programmatically or symmetrical which prevents the relative shift between the input and output signals. The trade-off for moving average filter design is easy to observe. Increasing the window size, increases the smoothing of the signal at the expense of response time to sharp changes in the input.

5.2.3 Median Filter

The next filter is the median filter. The median filter unlike the averaging filter is able to preserve sharp edges from isolated outliers while still handling local noise. It is shown in (14).

$$y[i] = median\{W_i^H\} = median\{x_{i-H}, \dots x_i, \dots, x_{i+H}\} \quad (14)$$

One issue with centered median filters is dealing with the boundaries of the signal. The method taken here was not processing the boundary and waiting until the window was filled. Padding the filter before a data stream is received could be implemented when testing future versions of this sensor while integrated into the whole system.

5.2.4 Kalman Filter

The last filter to be tested is the Kalman filter. The Kalman filter is a two stage, recursive process that estimates the state of the system based on a series of past measurements. The time discrete Kalman filter equations are split into the two stages. The first is the predict stage in (15) and (16).

$$\hat{x}_{k|k-1} = F_k \hat{x}_{k-1|k-s} + B_k u_k \quad (15)$$

$$P_{k|k-1} = F_k P_{k-1|k-1} F_k^T + Q_k \quad (16)$$

where $\hat{x}_{k|k-1}$ is the a priori state estimate for a posterior state $\hat{x}_k$, F_k is the state transition matrix, and B_k and u_k are the control matrix and control variables. P_k is the state variance matrix which is the covariance matrix a priori of the estimated error and Q_k is the process variance matrix which is the error due to the process. The Q_k matrix is one of the tuning parameters in optimizing the Kalman Filter. The second phase is the update which is composed of the three main equations.

$$\hat{x}_{k|k} = \hat{x}_{k|k-1} + K_k(y_k - H_k\hat{x}_{k|k-1}) \tag{17}$$

$$K_k = P_{k|k-1}H_k^T\left(H_kP_{k|k-1}H_k^T + R_k\right)^{-1} \tag{18}$$

$$P_{k|k} = (I - K_kH_k)P_{k|k-1} \tag{19}$$

where K_k is the optimal Kalman gain which minimizes the error covariance matrix of a posteriori. The R_k is the measurement error matrix which is another tuning parameter that can be found by finding the covariance of raw sensor measurements. The Kalman filter is made by modeling the state and measurement process. In this case, it is assumed to be a static model represented by a first order system. It was assumed that the measurement was the same scale as the state and the control variables were not used. This resulted in the parameters in Table 5.2.

Table 5.2 Kalman Filter Parameters

Kalman Filter Parameter (Scalars)	Symbol	Value (unit)
State Transition Matrix	F_k	1
Control Matrix	B_k	0
Control Variables	u_k	0
Measurement Matrix	H_k	1
Process Variance Matrix (Test Specific)	Q_k	[100, 1, 0.01]
Measurement Variance Matrix	R_k	3.7811

The R parameter was found using the variance of the measurements while the Q was found somewhat arbitrarily by calculating the covariance of a random range changing scenario and then

adjusting based on the first simulations. The initial Q was adjusted until it was within reason for performance comparison sake. The tuning parameters drive the filter performance; however, future work should incorporate an improved non-scalar model that accounts for the dynamics of the aerial vehicle and the other sensors in the error estimation (sensor fusion).

5.3 Additive Gaussian Noise Filtering Results

Three test scenarios were considered for the noise filters with two main performance measures. Filtering performance was analyzed for noise induced error reduction (improved accuracy) and filter response time to system state changes. The three range scenarios are shown in Table 5.3.

Table 5.3 Filter Test Scenarios

Scenario	Range (cm)
Fixed Range	300
Instantaneous Set Range Change	[275, 225, 350, 325]
Random Range Change	Nominal 300, Random 230:360

The fixed range measurement was for a steady state condition and the preset range changes and random range changes were for examining the filter response.

5.3.1 Filter Performance: Fixed Range

The result for the static test at a 300cm sensor range for all the filters are shown in Figure 5.7, Figure 5.8, and Figure 5.9. The top subplot shows the total measurements for 20 seconds with a measurement rate of 10 Hz. The bottom subplots show data magnified to a smaller 2 second time sample to observe the errors.

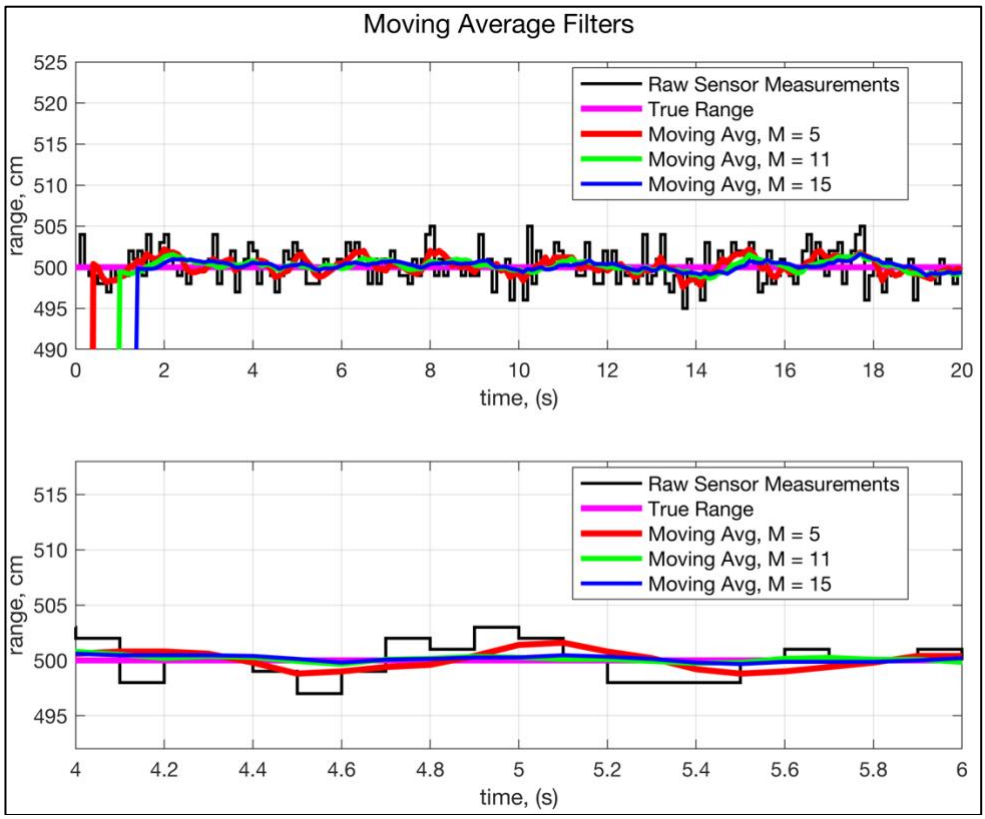

Figure 5.7 Moving Average Filter Results, Fixed Range

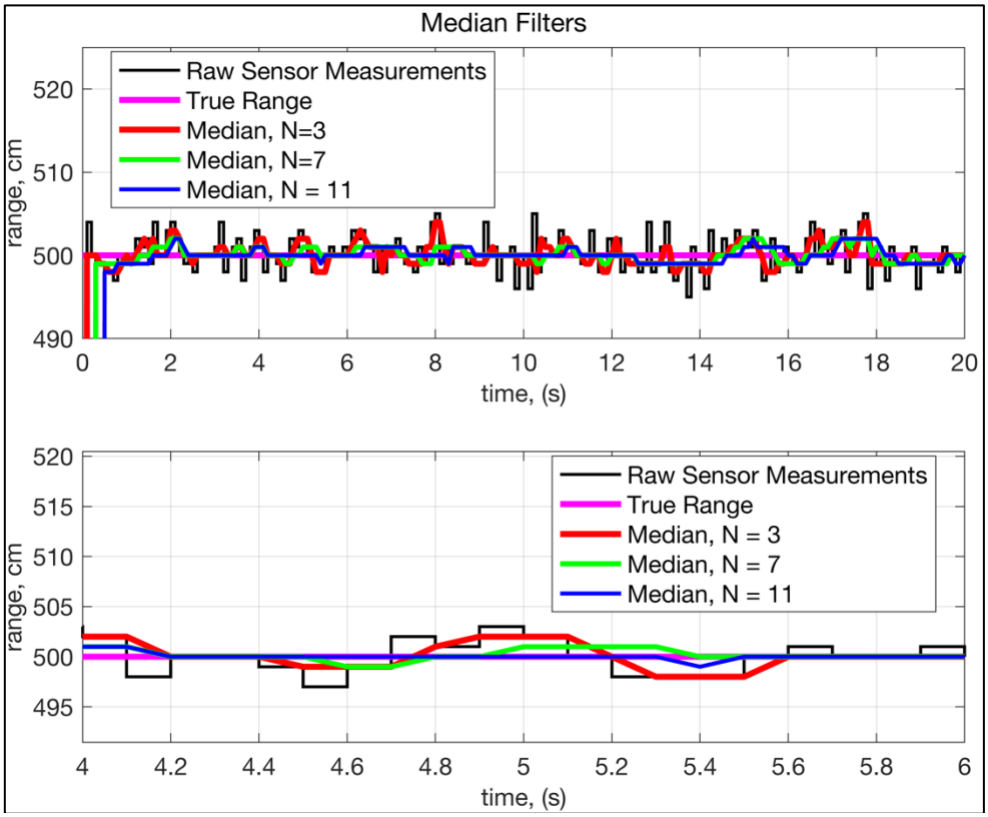

Figure 5.8 Median Filter Results, Fixed Range

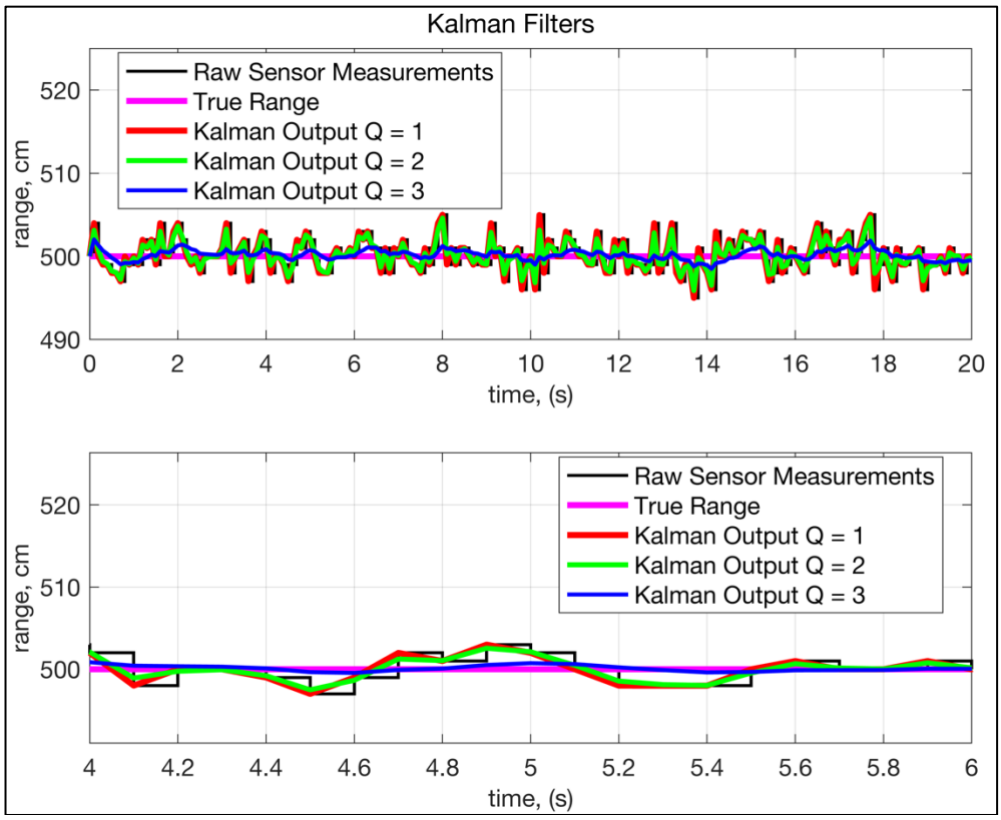

Figure 5.9 Kalman Filter Results, Fixed Range

One can see from the figures that the measurement errors are reduced as each respective filter's parameters are changed. The quantitative error results are shown in Table 5.4

Table 5.4 Filter Noise Reduction Results, Fixed Range

Filter Type	Error Statistics				
	RMS	90th %	Median	Mean	Variance
Moving Avg 5	0.978	1.000	0.000	-0.152	0.938
Moving Avg 11	0.648	0.636	-0.091	-0.147	0.400
Moving Avg 15	0.540	0.600	-0.200	-0.144	0.272
Median 3	1.314	1.000	0.000	-0.114	1.722
Median 7	0.912	1.000	0.000	-0.085	0.828
Median 11	0.858	1.000	0.000	-0.010	0.740
Kalman 1	1.939	1.996	0.000	-0.154	3.755
Kalman 2	1.584	1.756	-0.034	-0.155	2.497
Kalman 3	0.618	0.593	-0.180	-0.126	0.351

The assumption is then to increase the window size for the moving average and median filters and decrease the process variance for the Kalman filter. However, it will be seen in the second and third test scenarios that for a dynamic environment, there is an impact on the accuracy of the data due to delays in the filtering process.

5.3.2 Filter Performance: Instantaneous Range Change

The second scenario consisted of preset instantaneous range changes to observe the response to sharp changes. The result of the filters is shown in Figure 5.10, Figure 5.11, and Figure 5.12.

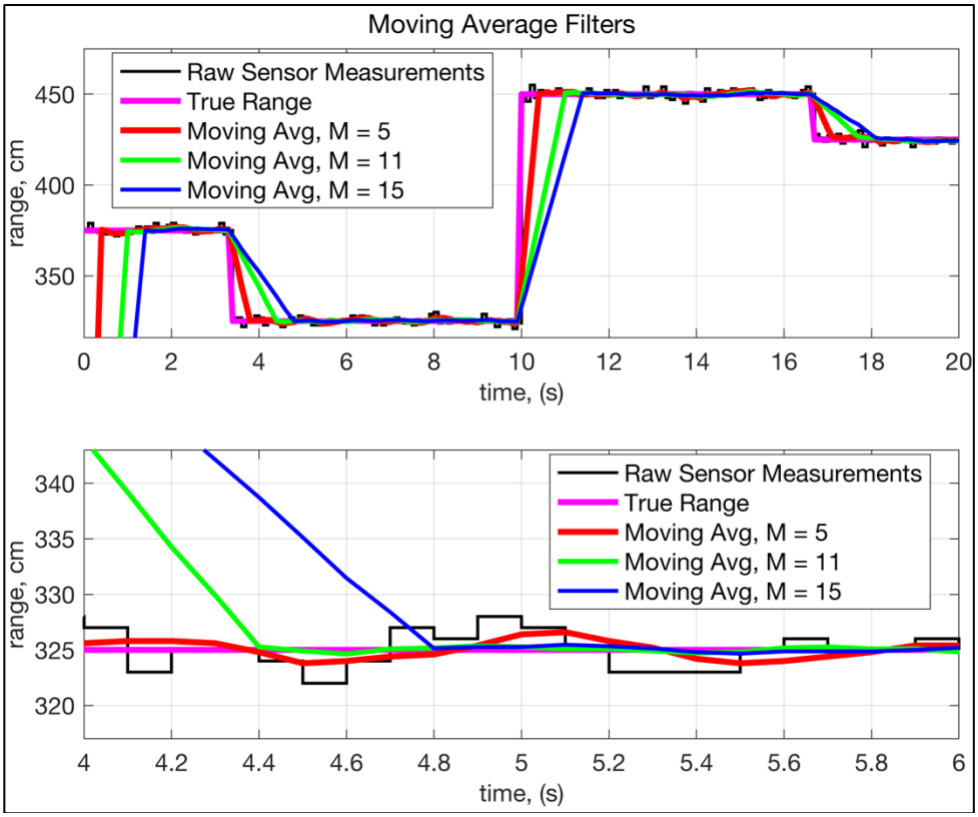

Figure 5.10 Moving Average Filter Results, Instantaneous Set Range Changes

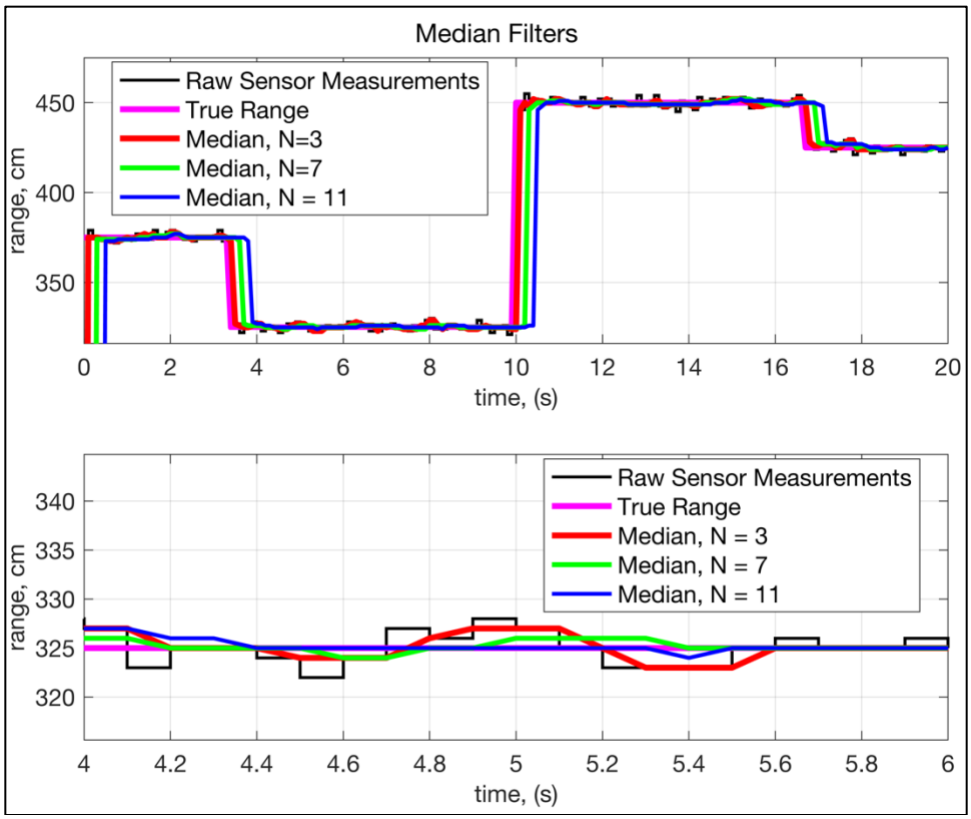

Figure 5.11 Median Filter Results, Instantaneous Set Range Changes

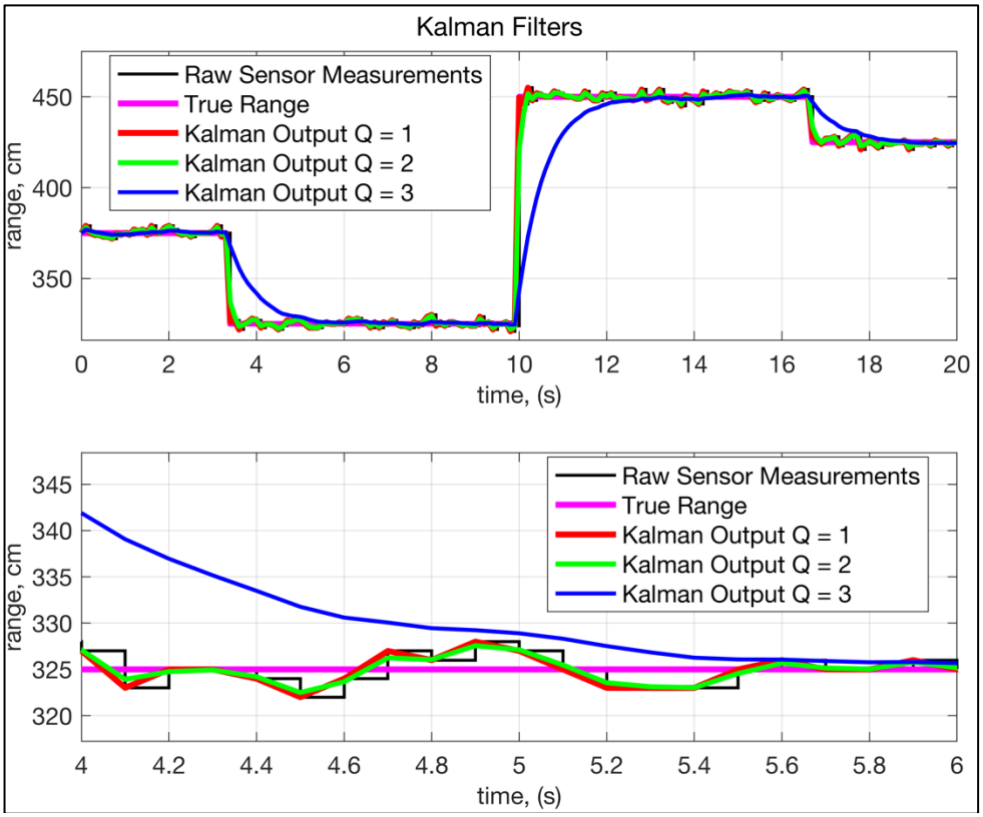

Figure 5.12 Kalman Filter Results, Instantaneous Set Range Changes

The response time is evident from the second scenario. The accuracy during the static case of the filter parameters is reversed by the slowed response to rapid range changes. The sharp edges increase the total error as shown in the range error statistics in Table 5.5.

Table 5.5 Filter Noise Reduction Results, Instantaneous Set Range Change

Filter Type	Error Statistics				
	RMS	90^{th} %	Median	Mean	Variance
Moving Avg 5	20.019	1.200	1.074	-0.200	401.606
Moving Avg 11	29.368	0.945	2.587	-0.182	860.070
Moving Avg 15	34.240	19.773	3.554	-0.333	1165.529
Median 3	1.353	1.000	-0.090	0.000	1.832
Median 7	0.987	1.000	-0.060	0.000	0.976
Median 11	1.007	1.000	0.000	0.000	1.020
Kalman 1	1.941	1.996	-0.153	0.000	3.762
Kalman 2	2.840	1.756	-0.082	-0.034	8.100
Kalman 3	15.692	4.304	1.233	-0.329	245.951

The specified range changes are sufficient for observing the response of the filters, yet, they are not representative of how the range measurements will actually occur.

5.3.3 Filter Performance: Random Range Changes

The third scenario looks at filter performance for randomly changing range measurements. The random ranges include sharp changes, smooth slopes, and very few instances of the measurements settling into a steady state condition. The filter performance results for this scenario are shown in Figure 5.13, Fig. 5.14., and Figure 5.15 respectively.

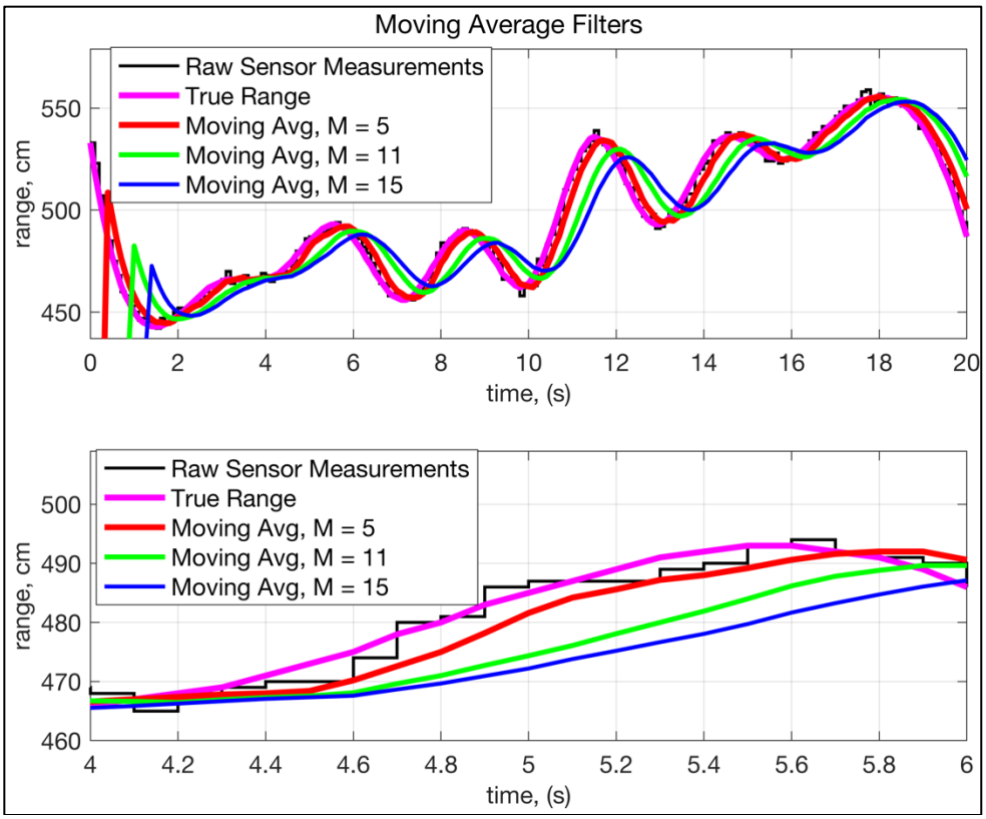

Figure 5.13 Moving Average Filter Results, Random Range Change

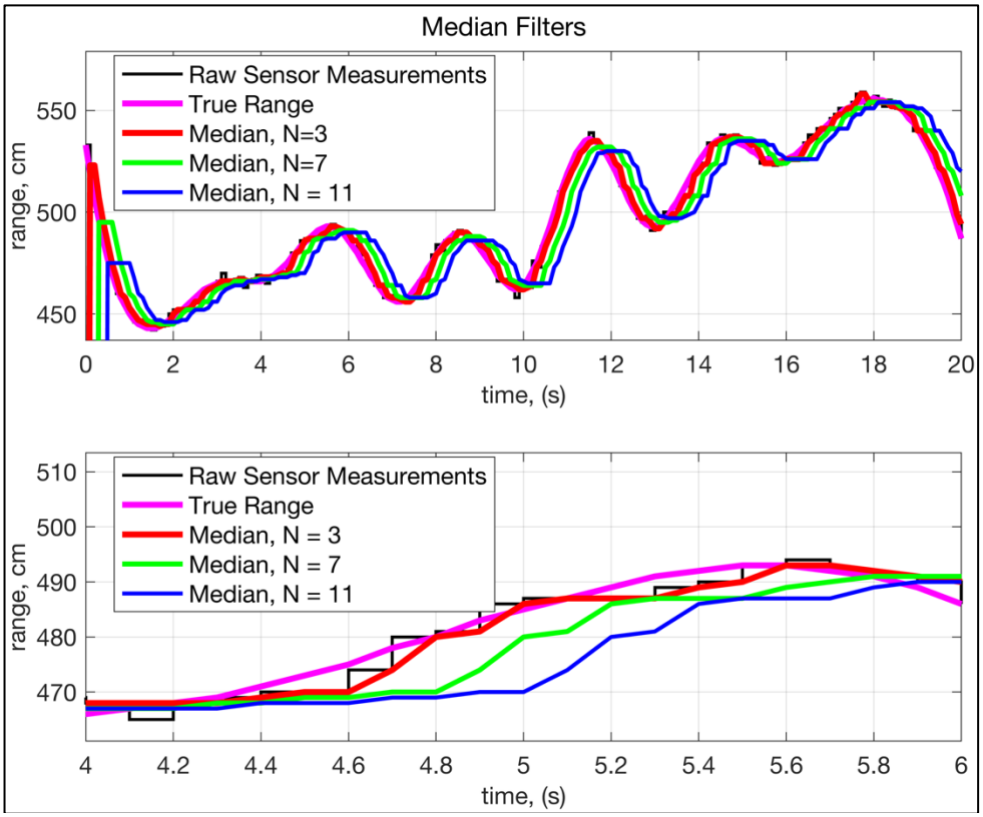

Figure 5.14, Median Filter Results, Random Range Change

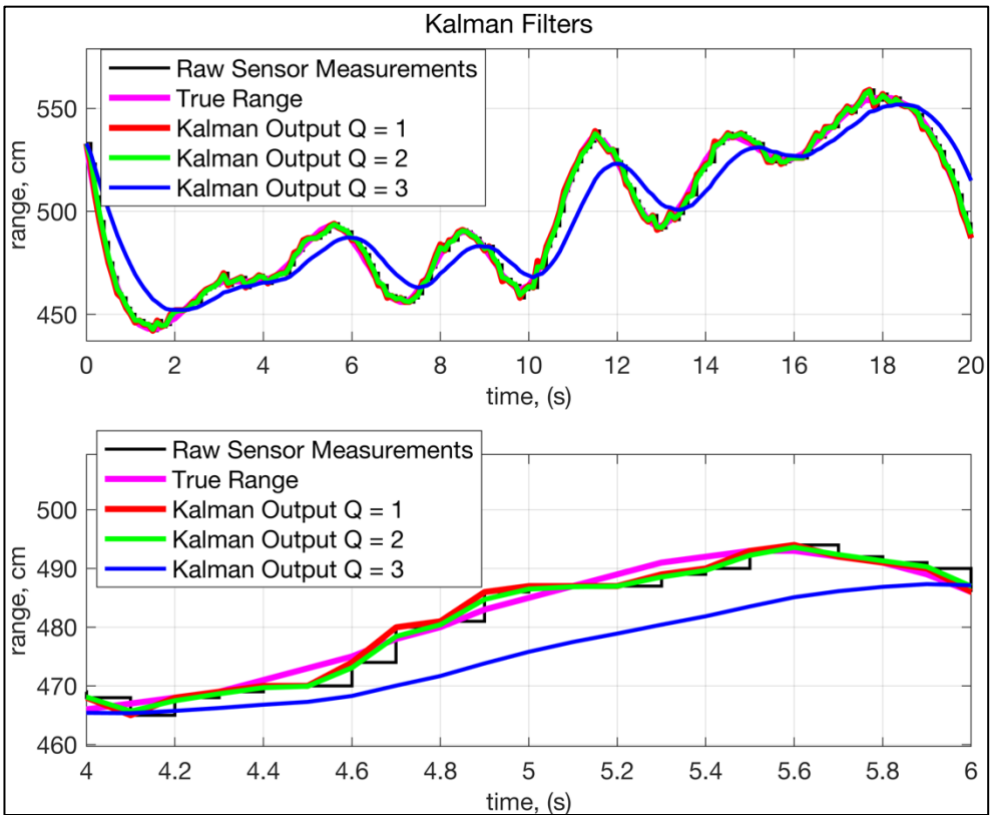

Figure 5.15 Kalman Filter Results, Random Range Change

The Kalman filter yields low error values for random range changes when using an increased Q value. The flight of an aerial vehicle can change rapidly. Higher process variance values should be assumed to compensate for it. The quantitative results for each filter for the random range measurements are shown in Table 5.6.

Table 5.6 Filter Noise Reduction Results, Random Range Change

	Error Statistics				
Filter Type	RMS	90th %	Median	Mean	Variance
Moving Avg 5	25.522	11.280	2.742	0.400	647.046
Moving Avg 11	45.286	29.855	6.979	1.091	2012.159
Moving Avg 15	55.317	40.373	9.824	1.800	2978.318
Median 3	1.690	2.000	-0.109	0.000	2.858
Median 7	1.981	2.000	0.015	0.000	3.945
Median 11	2.650	4.000	0.144	0.000	7.034
Kalman 1	1.939	2.002	-0.154	0.000	3.755

Kalman 2	2.014	2.136	-0.165	0.015	4.051
Kalman 3	16.724	20.031	-0.889	1.296	280.292

The moving average and median filters demonstrate similar performance between the specified and random range changes. The simplicity of the filters is sufficient for the basic scenarios. However, their performance cannot be improved much except for increasing the window size which was demonstrated to be proportional to the amount of delay in the response. The Kalman filter can be adjusted for each process variance. The result is reduced error with minimal delay. Future work should include analyzing an appropriate process covariance matrix in addition to improving the Kalman filter model.

Chapter 6: Conclusion

The performance characterization of a range finding sensor was successful. Range finding data was collected for a variety of test conditions including at maximum range, with varying incidence angles, with varying target materials, in fluctuating temperatures, on a vibrating platform, and in the presence of other ultrasonic transmitters. The sensor behavior was analyzed for each test condition by calculating the range errors under the influence of each factor. The temperature, incidence angle, and simultaneous ultrasonic sensor operations affected the range accuracy the most. Several preliminary data processing measures improved the ranging accuracy for a stationary target. Compensating for temperature fluctuations reduced the sensing errors in real time. Three filters were evaluated to determine which was most effective for gaussian measurement noise. Experimental results demonstrated that the median filter was most effective for improving accuracy, however, the Kalman filter had a faster response with more potential by tuning the covariance parameters. Completing these tasks means that all sub-objectives were met and the goal of this project was accomplished. Potential future work for this project includes applying this characterization approach to the other sensors on the Drone MSP such as the radar and lidar. Additionally, a higher fidelity model for the Kalman filter could be implemented for an ultrasonic sensor in a dynamic environment or an extended Kalman filter can be used to integrate the data streams of all of the range finding sensors.

References

[1] A. Carmona, D. Chitella, M. Giron, Y. Goudjil, M. Hossain, O. Tejeda, R. Tejuco, and J. Villalobospineda, “Sensor Hardware Fusion for Increasing Trusted Autonomy,” Apr. 2020.

[2] L. Gipson, “Advanced Air Mobility (AAM),” NASA, 02-Aug-2019. [Online]. Available: https://www.nasa.gov/aam. [Accessed: 01-Jul-2020].

[3] MaxBotix, “I2CXL-MaxSonar®- EZ™ Series High Performance Sonar Rangefinder,” MB1242 datasheet, 2012.

[4] D. A. Timucin, "A Bayesian approach to sensor characterization," IGARSS 2003. 2003 IEEE International Geoscience and Remote Sensing Symposium. Proceedings (IEEE Cat. No.03CH37477), Toulouse, 2003, pp. 3775-3777 vol.6, doi: 10.1109/IGARSS.2003.1295266.

[5] C. G. Raghavendra, S. Akshay, P. Bharath, M. Santosh and D. Vishwas, "Object tracking and detection for short range surveillance using 2D ultrasonic sensor array," 2016 International Conference on Circuits, Controls, Communications and Computing (I4C), Bangalore, 2016, pp. 1-4, doi: 10.1109/CIMCA.2016.8053267.

[6] V. Kunin, W. Jia, M. Turqueti, J. Saniie and E. Oruklu, "3D direction of arrival estimation and localization using ultrasonic sensors in an anechoic chamber," 2011 IEEE International Ultrasonics Symposium, Orlando, FL, 2011, pp. 756-759, doi: 10.1109/ULTSYM.2011.0184.

[7] G. Găşpăresc and A. Gontean, "Performance evaluation of ultrasonic sensors accuracy in distance measurement," 2014 11th International Symposium on Electronics and Telecommunications (ISETC), Timisoara, 2014, pp. 1-4, doi: 10.1109/ISETC.2014.7010761.

[8] H. Zhao and Z. Wang, "Motion Measurement Using Inertial Sensors, Ultrasonic Sensors, and Magnetometers With Extended Kalman Filter for Data Fusion," in IEEE Sensors Journal, vol. 12, no. 5, pp. 943-953, May 2012, doi: 10.1109/JSEN.2011.2166066.

[9] N. A. Singh and M. Borschbach, "Effect of external factors on accuracy of distance measurement using ultrasonic sensors," 2017 International Conference on Signals and Systems (ICSigSys), Sanur, 2017, pp. 266-271, doi: 10.1109/ICSIGSYS.2017.7967054.

[10] Liao, Xiaoqun & Hall, Ernest. (1999). A Probabilistic Model for AGV Mobile Robot Ultrasonic Sensor. 10.1117/12.360291.

[11] Tahtawi, A. R. A.. “Kalman Filter Algorithm Design for HC-SR04 Ultrasonic Sensor Data Acquisition System.” 2018.

[12] A. Raghavan, “Sensor Performance Characterization for Use on a Micro Aerial Vehicle.”

[13] S. Khubchandani, M. R. Hodkiewicz and A. Keating, "Characterizing the Performance of LED Reflective Distance Sensors," in IEEE Access, vol. 5, pp. 14289-14297, 2017, doi: 10.1109/ACCESS.2017.2731801.

[14] S. M. Howard, “Deep Learning for Sensor Fusion,” Aug. 2017.

[15] D. P. Massa, “Understanding How Frequency, Beam Patterns of Transducers, and Reflection Characteristics of Targets Affect the Performance of Ultrasonic Sensors,” Massa Products Corporation.

[16] M. D. Fletcher, S. L. Jones, and P. R. White, “Public exposure to ultrasound and very high-frequency sound in air,” The Journal of the Acoustical Society of America, Oct. 2018.

[17] “Ultrasonic Transducer Technical Notes,” Olympus NDT.

[18] S. Thrun, W. Burgard, and D. Fox, Probabilistic robotics. Cambridge, MA: The MIT Press, 2006.

[19] Zhang, Hongjuan & Wang, Yu & Zhang, Xu & Wang, Dong & Jin, Baoquan. (2016). Design and Performance Analysis of an Intrinsically Safe Ultrasonic Ranging Sensor. Sensors. 16. 867. 10.3390/s16060867.

[20] J. Taghipour, “The Effect of Filtering on Proximity Sensors,” 2017.

[21] “Kalman Filter Applications,” Cornell - Computer Science, Sep. 2008.

[22] D. G. Davies, R. C. Bolam, Y. Vagapov and P. Excell, "Ultrasonic sensor for UAV flight navigation," 2018 25th International Workshop on Electric Drives: Optimization in Control of Electric Drives (IWED), Moscow, 2018, pp. 1-7, doi: 10.1109/IWED.2018.8321389.

[23] Sasidharan, Adarsh & Salahuddin, Mohamed Kaleemuddin & Bose, Dinesh & Ramachandran, K. (2016). Performance comparison of Infrared and Ultrasonic sensors for obstacles of different materials in vehicle/ robot navigation applications. IOP Conference Series: Materials Science and Engineering. 149. 012141. 10.1088/1757-899X/149/1/012141.